



Recurrent architecture for adaptive regulation of learning in the insect brain

Claire Eschbach^{1,2,13}, Akira Fushiki^{1,3,13}, Michael Winding^{1,2}, Casey M. Schneider-Mizell^{1,4}, Mei Shao¹, Rebecca Arruda¹, Katharina Eichler^{1,5}, Javier Valdes-Aleman¹, Tomoko Ohyama^{1,6}, Andreas S. Thum^{1,7}, Bertram Gerber^{1,8}, Richard D. Fetter¹, James W. Truman^{1,9}, Ashok Litwin-Kumar¹⁰ ✉, Albert Cardona^{1,11,12} ✉ and Marta Zlatic^{1,2,11} ✉

Dopaminergic neurons (DANs) drive learning across the animal kingdom, but the upstream circuits that regulate their activity and thereby learning remain poorly understood. We provide a synaptic-resolution connectome of the circuitry upstream of all DANs in a learning center, the mushroom body of *Drosophila* larva. We discover afferent sensory pathways and a large population of neurons that provide feedback from mushroom body output neurons and link distinct memory systems (aversive and appetitive). We combine this with functional studies of DANs and their presynaptic partners and with comprehensive circuit modeling. We find that DANs compare convergent feedback from aversive and appetitive systems, which enables the computation of integrated predictions that may improve future learning. Computational modeling reveals that the discovered feedback motifs increase model flexibility and performance on learning tasks. Our study provides the most detailed view to date of biological circuit motifs that support associative learning.

To behave adaptively in an ever-changing environment, animals must be able to learn new associations between sensory cues (conditioned stimuli, CS) and rewards or punishments (aversive and appetitive unconditioned stimuli, US), and continuously update previous memories, depending on their relevance and reliability^{1–3}.

Modulatory neurons (for example, DANs) convey information about rewards and punishments, and provide the teaching signals for updating the valence associated with CS in learning circuits across the animal kingdom (for example, the vertebrate basal ganglia^{1,4} or the insect mushroom body, MB)^{3,5,6}. The co-occurrence of CS and modulatory neuron activity tuned only to the received US can support simple associative memory formation⁶. To account for more complex behavioral phenomena, theories have been developed in which learning can be regulated by previously formed associations^{7,8}. According to reinforcement learning theories, learning is driven by errors between predicted and actual US (prediction errors)^{7,8}, which are thought to be represented by the activity of DANs^{1,4}. Indeed, in many model organisms, the responses of modulatory neurons have been shown to be adaptive, including monkeys¹, rodents^{4,9} and insects^{3,5,10,11}. Despite recent progress^{3,4,9}, the basic principles by which DAN activity is adaptively regulated and teaching signals are computed are not well understood.

A prerequisite for the adaptive regulation of modulatory neuron activity is convergence of afferent pathways that convey information about received US^{1,4} with feedback pathways that convey information about previous experiences. A comprehensive

synaptic-resolution connectivity map of the feedback circuits that regulate modulatory neurons would provide a basis for understanding how learning is adaptively regulated by prior learning, but it has previously been out of reach.

Insects, especially in their larval stages, have small and compact brains that have recently become amenable to large-scale electron microscopy (EM) circuit mapping^{12,13}. Both adult^{3,6,14} and larval¹⁵ insect stages possess a brain center that is essential for associative learning, the MB. The MB contains neurons called Kenyon cells (KCs) that sparsely encode CS, MB modulatory neurons (collectively called MB input neurons, MBINs) that provide the teaching signals and MB output neurons (MBONs) whose activity represents learnt valences of stimuli^{3,6,14,15}. In the *Drosophila* larva, most modulatory neurons are DANs, some are octopaminergic neurons (OANs) and some have unidentified neurotransmitters (simply called MBINs)¹⁵. Modulatory neurons and MBONs project axon terminals and dendrites, respectively, onto the KC axons in a tiled manner, defining MB compartments, in both adult³ and larval¹⁵ *Drosophila*. In adult *Drosophila*, it has been shown that coactivation of KCs and DANs reduces the strength of the KC–MBON synapse in that compartment^{3,16,17}. Different compartments have been implicated in the formation of distinct types of memories, for example, aversive and appetitive, or short and long term^{3,14,15,18,19}. However, despite a good understanding of the structure and function of the core components of the MB in both adult^{3,6,14,20} and larval *Drosophila*¹⁵, the circuits presynaptic to modulatory neurons that regulate their activity have remained relatively uncharacterized.

¹HIMI Janelia Research Campus, Ashburn, VA, USA. ²Department of Zoology, University of Cambridge, Cambridge, UK. ³Departments of Neuroscience and Neurology, Zuckerman Mind Brain Behavior Institute, Columbia University, New York, NY, USA. ⁴Allen Institute for Brain Science, Seattle, WA, USA. ⁵Institute of Neurobiology, University of Puerto Rico Medical Science Campus, San Juan, Puerto Rico, USA. ⁶Department of Biology, McGill University, Montreal, Quebec, Canada. ⁷Department of Genetics, Institute for Biology, University of Leipzig, Leipzig, Germany. ⁸Abteilung Genetik von Lernen & Gedächtnis, Leibniz Institut für Neurobiologie, Otto von Guericke University Magdeburg, Institut für Biologie, Verhaltensgenetik, & Center for Behavioral Brain Sciences, Magdeburg, Germany. ⁹Department of Biology, University of Washington, Seattle, WA, USA. ¹⁰Department of Neuroscience, Zuckerman Mind Brain Behavior Institute, Columbia University, New York, NY, USA. ¹¹MRC Laboratory of Molecular Biology, Cambridge, UK. ¹²Department of Physiology, Development & Neuroscience, University of Cambridge, Cambridge, UK. ¹³These authors contributed equally: Claire Eschbach and Akira Fushiki. ✉e-mail: ak3625@columbia.edu; acardona@mrc-lmb.cam.ac.uk; mzlati@mrc-lmb.cam.ac.uk

We therefore reconstructed all neurons presynaptic to all modulatory neurons in an EM volume that spans the entire nervous system of a first instar *Drosophila* larva, in which we had previously reconstructed all the core components of the MB¹². We also determined which individual modulatory neurons are activated by punishments and reconstructed their afferent US pathways from nociceptive and mechanosensory neurons. We characterized the neurotransmitter profiles of some of the neurons in the network and functionally confirmed some of the identified structural connections. Finally, we developed a model of the circuit constrained by the connectome, the neurotransmitter data and the functional data, and used it to explore the computational advantages offered by the recently discovered architectural motifs for performing distinct learning tasks.

Results

Larval MB modulatory neurons for aversive and appetitive memory formation. We began with a functional characterization of larval modulatory neurons and asked which ones signal punishment or reward. Activation of all DL-cluster DANs that target the vertical lobe, the lateral appendix and the peduncle (with a broadly expressing TH-GAL4 driver line) has been shown to induce aversive memory for paired odors²¹. Activation of individual larval PAM-cluster DANs that target the MB medial lobe has been shown to induce appetitive memory for paired odors²². However, the role of other individual modulatory neuron types was not known. We generated Split-GAL4 lines that drive expression selectively in one or two modulatory neurons per hemisphere (Fig. 1a, Extended Data Fig. 1 and Supplementary Table 1).

We then paired an odor (CS) with optogenetic activation of these modulatory neurons in a three-trial, one-odor, short-term memory associative memory paradigm (Fig. 1b). We found that activation of DAN-f1 (innervating the intermediate vertical lobe), DAN-g1 (lower vertical lobe) or DAN-d1 (lateral appendix) established aversive memory for paired odors (Fig. 1c and Extended Data Fig. 2). In contrast, as previously reported^{15,22}, activation of DANs that innervate the medial lobe led to the formation of an appetitive memory for paired odors (Fig. 1c and Extended Data Fig. 2). Thus, similar to findings in the adult fly^{3,18}, larval DANs that innervate distinct lobes signal opposite valences.

Pairing of an odor with the activation of DAN-c1 (lower peduncle) or of the non-dopaminergic modulatory neurons induced neither appetitive nor aversive memory (Fig. 1c and Extended Data Fig. 2). Thus, our analysis revealed at least three functionally distinct classes of compartments in the larval MB: medial lobe compartments whose DANs can induce appetitive memory for paired odors, lateral appendix and lower and intermediate vertical lobe compartments whose DANs can induce aversive memory for paired odors, and others whose modulatory neurons were not sufficient to induce short-term memory (Fig. 1c).

Punishment encoding across larval MB modulatory neurons. Next, we asked whether there is any functional diversity within the population of DANs whose activation signals punishment.

Larvae sense multiple types of innately aversive somatosensory stimuli that evoke distinct types of innate avoidance and escape responses^{23–27} (Fig. 1d). Already the mildest of these punishments, vibration that is transduced by mechanosensory neurons evokes a turning avoidance response and induces aversive memory for paired odors²⁸. Fittingly, we found that optogenetic activation of nociceptive sensory neurons and of Basin interneurons (and their downstream A00c interneurons) that evokes more vigorous fast crawling and rolling escape, respectively, also induces aversive memory for paired odors (Fig. 1d,e and Extended Data Fig. 2).

We therefore asked how individual modulatory neurons respond to different punishment types by monitoring their calcium

transients in response to optogenetic activation of specific somatosensory neurons. In each of the three DANs whose activation induced aversive memory for paired odors, we found reliable responses to at least two fictive punishment types. Each punishment type evoked reliable and statistically significant responses in at least two DANs, but each DAN's tuning differs (Fig. 1f). Thus, these three DANs could combinatorially encode punishment type or salience.

For comparison, we also tested responses of a few modulatory neurons (e.g., of upper vertical lobe, UVL) whose activation paired with odor did not induce short-term aversive memory, and found that they were not significantly activated by the fictive punishments (Fig. 1f).

EM reconstruction of all input neurons to MB modulatory neurons. To provide a basis for understanding how the activity and function of modulatory neurons are regulated, we sought to comprehensively identify all of the neurons presynaptic to them. We have previously reconstructed all of the KCs, MBONs and modulatory neurons in an EM volume of a first instar larval nervous system¹². Here, we systematically reconstructed all neurons presynaptic to all modulatory neurons (that is, premodulatory neurons) in the same EM volume (Fig. 2a–e). We identified 213 left-right homologous pairs and 5 unpaired premodulatory neurons. Of these, 102 homologous pairs were reliably and strongly connected (see Methods; Fig. 2a,b,e; Supplementary Adjacency Matrices 1, 2 and 3; and Supplementary Atlas). Although the 'other weakly connected partners' could also influence modulatory neuron activity, especially in combination with each other, we focus our study mainly on the 102 reliably and strongly connected partners.

We asked how the functional diversity of modulatory neurons relates to their input diversity. As expected, functionally distinct DANs receive inputs from distinct subsets of premodulatory neurons, and functionally similar DANs share a higher fraction of presynaptic partners with each other than with other DANs (Fig. 2e and Extended Data Fig. 3). Nevertheless, each modulatory neuron type, which is distinguishable based on the compartment it innervates or based on neurotransmitter expression, receives input from a unique combination of neurons, and thus potentially encodes a unique set of features.

Feedback neurons reveal a highly recurrent architecture for computing teaching signals. We aimed to characterize the premodulatory neurons based on the inputs they receive. We asked whether they convey information about previously formed memories (via feedback originating from MBONs) or about received US (via afferent input from sensory neurons), or both. Surprisingly, we found that the majority (61/102) of premodulatory neurons receive feedback input from MBONs (Fig. 2a–c and Extended Data Fig. 4a–c). Forty neuron pairs receive reliable direct input from MBONs, providing one-step feedback from MBONs to modulatory neurons (we call these one-step feedback neurons (FBNs); Fig. 2a–c and Extended Data Fig. 4a). Another 21 premodulatory neuron pairs receive reliable direct input from FBNs (but not MBONs) and provide two-step feedback from MBONs (two-step feedback neurons (FB2Ns); Fig. 2a–c and Extended Data Fig. 4b). The majority of FBNs also receive input from other FBNs, providing two-step, as well as one-step, feedback (Fig. 2b,c and Extended Data Fig. 4a). The remaining premodulatory neurons do not receive reliable direct MBON or FBN input, so we classified them tentatively as 'feedforward neurons' (FFNs; Fig. 2a–c).

To determine the likelihood that MBONs could influence modulatory neuron activity via the feedback pathways, we analyzed the fraction of total input that FBNs and FB2Ns receive from MBONs and that modulatory neurons receive from feedback pathways. In previous studies we have demonstrated functional connections when neurons received 2% or more of their input from another

FBN and FB2N activity. Strikingly, we found that many modulatory neurons receive more than 50% of their total dendritic input from all feedback pathways combined (Fig. 2d). This suggests that modulatory neuron activity could be strongly influenced by MBON activity.

Multilevel convergence of afferent and feedback pathways. We investigated how the feedback pathways from MBONs converge with afferent pathways from US sensing neurons. We focused on the DANs that respond to somatosensory neuron activation (Fig. 1f) and asked whether they receive somatosensory and MBON input via distinct or overlapping premodulatory neurons. We had previously reconstructed all first-order neurons downstream of nociceptive and mechanosensory sensory neurons and a subset of second- and third-order ones^{26,27}. This enabled us to search for the shortest pathways from these somatosensory neurons to modulatory neurons. Although the pathways identified in this way represent only a subset of existing pathways, nevertheless, we were able to identify two-, three- and four-step pathways from the somatosensory neurons to six different premodulatory neurons that target the vertical lobe and lateral appendix modulatory neurons: three FFNs and three FB2Ns (Fig. 2f, Supplementary Fig. 1, Supplementary Adjacency Matrix 1 and Supplementary Atlas). Thus, the afferent US pathways converge with feedback pathways from MBONs at multiple levels, both onto the modulatory neurons themselves (via FFNs) and onto the premodulatory FB2Ns.

Modulatory neurons receive convergent one-step feedback from multiple MBONs innervating functionally distinct compartments. Next, we analyzed in more detail the types of one-step feedback motifs formed by FBNs (Figs. 2a–c and 3a–c; Extended Data Figs. 5–9; Supplementary Fig. 2a,b; Supplementary Adjacency Matrix 1 and Supplementary Atlas). We observed a surprising diversity of one-step FBNs that linked unique combinations of MBONs with unique combinations of modulatory neurons (see Fig. 3a for examples and Extended Data 5 for the complete dataset). Out of the 40 FBNs, 7 provide exclusively within-compartment feedback, and 13 provide exclusively cross-compartment feedback. Interestingly, many FBNs (17; Fig. 3a,d, Extended Data Fig. 5 and Supplementary Fig. 2a) integrate input from MBONs of functionally distinct compartments (Fig. 1c and Extended Data Fig. 6). Almost all of these FBNs (at least 13/17) receive GABAergic (inhibitory) or glutamatergic (potentially also inhibitory^{29,30} in insects) input from MBONs innervating compartments and cholinergic (excitatory) inputs from MBONs innervating other compartments (Fig. 3a,d, Extended Data Fig. 5 and Supplementary Fig. 2a). The integration of inhibitory and excitatory inputs may enable these FBNs to more accurately read out the results of learning-induced plasticity by comparing its effects across compartments.

Not only do most FBNs receive input from multiple MBONs, but also most modulatory neurons receive input from multiple

FBNs (Figs. 2e and 3a, Extended Data Fig. 7 and Supplementary Fig. 2b). We therefore analyzed one-step connections from all MBONs to all modulatory neurons via FBNs. We found that most modulatory neurons receive one-step feedback from many MBONs and from each of the three functionally distinct regions of the MB: upper vertical lobe (unknown function), vertical lobe aversive memory compartments and medial lobe appetitive memory compartments (Fig. 3b,c). This is in stark contrast with the direct connections from MBONs to modulatory neurons, which are sparse and connect few compartments (Extended Data Fig. 8a,b). Thus, the recently discovered FBNs greatly increase the connectivity between MBONs and modulatory neurons, enabling the output from functionally distinct regions of the MB to influence the activity of single modulatory neurons during memory formation.

A modulatory neuron receives inhibitory and excitatory feedback from compartments of opposite valence. To gain a better understanding of the way in which feedback motifs influence modulatory neuron activity, we were able to determine the neurotransmitter profiles of some of them (see Methods). We found that four of the tested FBNs are cholinergic (that is, excitatory), three are GABAergic (that is, inhibitory) and one is glutamatergic (likely also inhibitory^{29,30}; Fig. 3a and Extended Data Fig. 9).

For a few cases where we could identify the neurotransmitter profiles of both the MBON¹² and the FBN in a one-step feedback connection, we predicted the signs of these connections (Fig. 3b). Of these, all of the true within-compartment feedback connections are potentially inhibitory (4/4), comprising a GABAergic or glutamatergic MBON and an excitatory FBN (Fig. 3b,e). In contrast, most of the (8/11) cross-compartment connections seem functionally excitatory, either disinhibitory (comprising an inhibitory MBON and an inhibitory FBN) or excitatory (comprising an excitatory MBON and an excitatory FBN; Fig. 3b,e). Furthermore, some modulatory neurons (for example, DAN-g1 and DAN-i1) receive both potentially inhibitory feedback from their own compartment and potentially excitatory feedback from compartments of opposite valence (Fig. 3b,e).

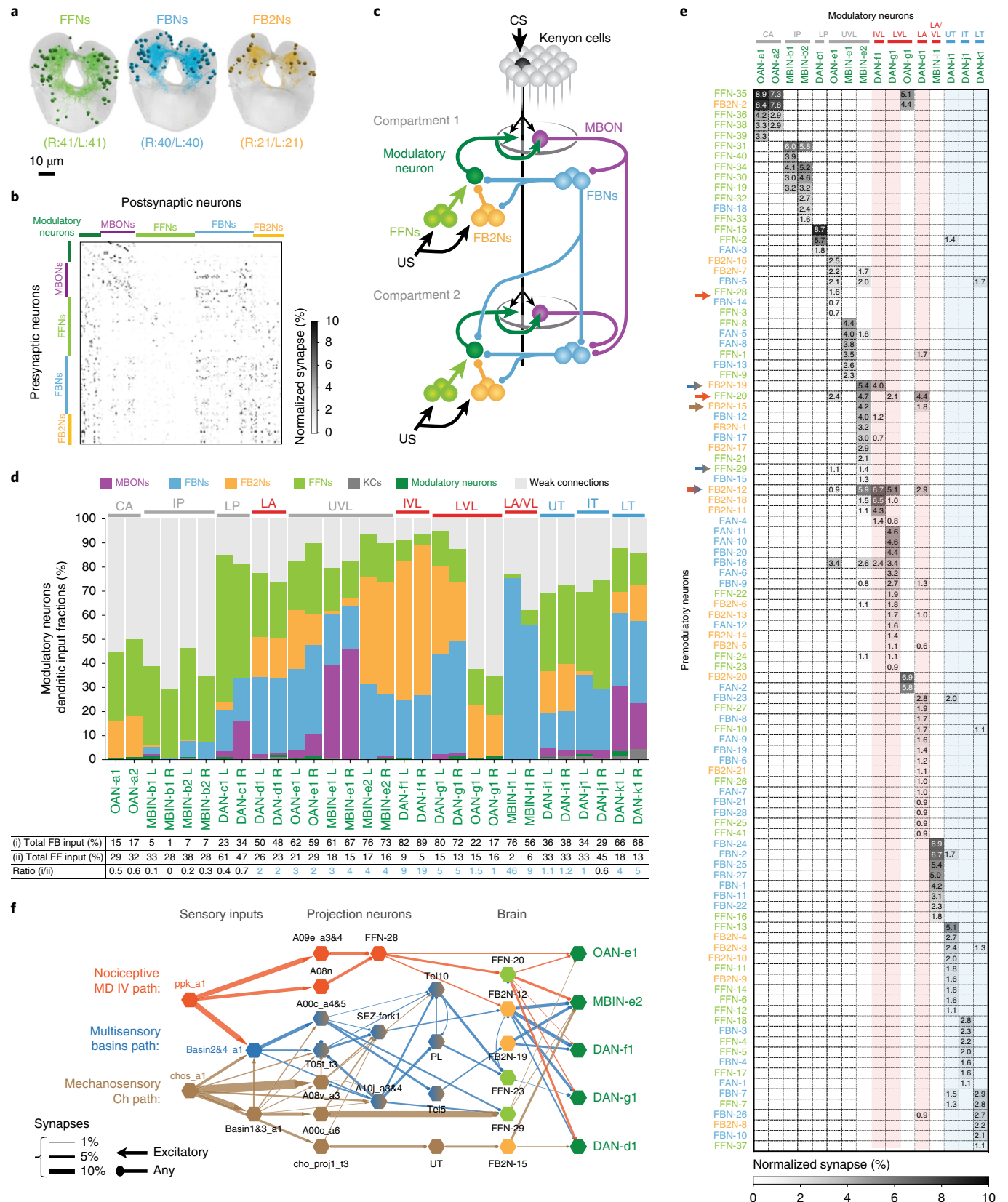
We wanted to functionally confirm the two types of predicted feedback connections onto the same DAN (Figs. 3e and 4a–g). DAN-i1 potentially receives inhibitory one-step feedback from MBON-i1 in its own compartment (Fig. 4a,b) and disinhibitory one-step feedback from MBON-m1 from compartments of opposite valence (Fig. 4a,e). Neither of these MBONs synapses directly onto DAN-i1. Furthermore, DAN-i1 receives two-step feedback from MBON-i1, but not from MBON-m1 (Fig. 5e). We activated these MBONs optogenetically while recording intracellularly from DAN-i1.

Activating MBON-i1 evoked long-latency (55 ± 17 ms) inhibitory responses in DAN-i1 in three of nine animals (Fig. 4c,d and Supplementary Fig. 3a), consistent with a polysynaptic connection

Fig. 2 | Comprehensive EM reconstruction of premodulatory neurons reveals a multilayered recurrent architecture for regulating learning. **a**, Projections of EM reconstructions of 102 neuron pairs found to be strongly connected to modulatory neurons. The majority (61) relays inputs from MBONs: 40 FBN pairs (light blue) and 21 FB2Ns (yellow). The remaining 41 are classified as FFNs (light green). **b**, Connectivity matrix showing normalized synaptic input (in %) each homologous pair of postsynaptic (columns) neurons receives from each pair of presynaptic (rows) neurons. **c**, Schematic wiring diagram of the extended MB circuit. **d**, Fraction of total dendritic input each modulatory neuron receives from different neuron types. Most DANs receive more than half of their input from MBON feedback pathways, whereas most OANs receive most input from weakly connected partners. Some DANs extend dendritic arbors to the KCs, which accounts for KCs dendritic input; KCs axonic inputs are described elsewhere (Eichler et al.¹²). Red and blue, aversive and appetitive memory compartments, respectively, in all legends. Bottom: percent of inputs onto modulatory neurons from (i) MBON, FBN, and FB2N; (ii) FFNs; and their ratio. This ratio is greater than 1 in most cases. **e**, Connectivity matrix showing normalized synaptic input (expressed as % input) each modulatory neuron (columns) receives from each premodulatory neuron (rows). Premodulatory neurons synapse onto a single or a few functionally related modulatory neuron(s) (see also Extended Data Fig. 3). VL, vertical lobe. **f**, US pathways converge with feedback pathways at modulatory neurons and at FB2Ns. Diagram shows the shortest identified US pathways from somatosensory neurons to vertical lobe modulatory neurons. Thickness of the arrow represents fraction of input.

mediated by an FBN (Figs. 3b and 4b). The interanimal variability could be caused by different baseline activity levels of the FBN (as illustrated in Supplementary Fig. 3b). In five of nine animals (Fig. 4c and Supplementary Fig. 3a) we observed inhibitory

responses to the offset of MBON-i1 activation only. These offset responses had a longer latency (95 ± 44 ms) than the onset responses and could therefore be mediated by a longer two-step feedback pathway (see Supplementary Fig. 3c).



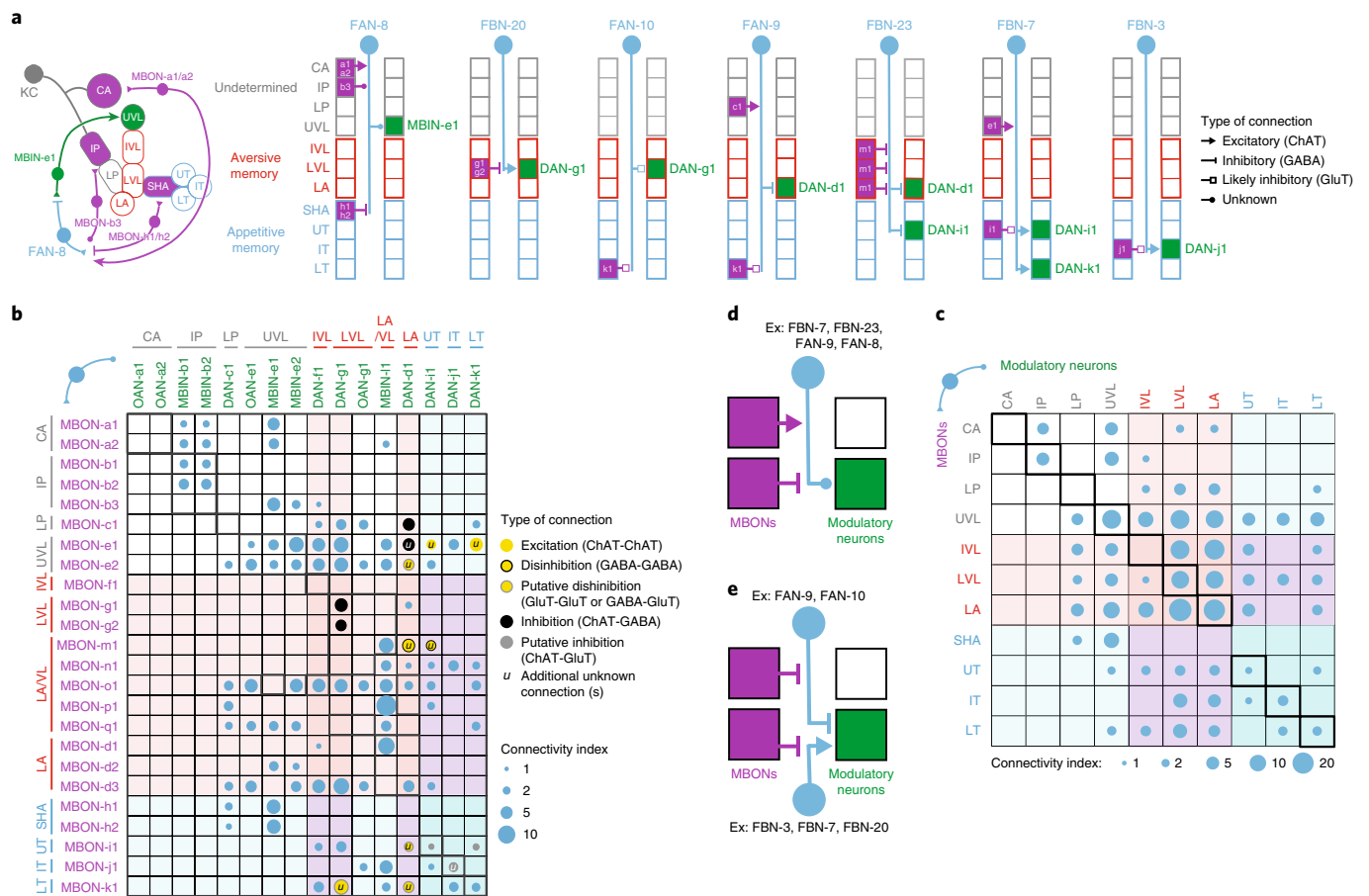


Fig. 3 | Modulatory neurons receive convergent one-step feedback from multiple MBONs from functionally distinct compartments. **a**, Diagram representing the connectivity of seven example pairs of homologous FBNs. Boxes indicate separate MB compartments, with presynaptic MBON(s) on the left side and postsynaptic modulatory neuron(s) on the right. When known (Extended Data Fig. 9 and Eichler et al.¹²), the neurotransmitter profiles of the MBONs and FBNs are indicated by the type of arrow. See Extended Data Fig. 5 for diagrams of each of the 40 FBNs. **b**, Connectivity matrix shows the one-step feedback connections between MBONs and modulatory neurons via FBNs, obtained by multiplying the MBON → FBN and FBN → modulatory neuron normalized connectivity matrices. Connectivity indexes are the square roots of the matrix products. Colored circles indicate putative signs of connections if neurotransmitters of both MBONs and FBN(s) are known. Red and blue color shades indicate aversive and appetitive compartments, respectively. Pure within-compartment connections (excluding multicompartment MBONs) are boxed in bold. The four pure within-compartment connections with known neurotransmitters are potentially inhibitory, in contrast with cross-compartment connections. **c**, Connectivity indexes from **b** pooled per compartment. **d, e**, Summary diagram of commonly observed convergence motifs. **d**, Many FBNs (at least 13) receive convergent inputs of opposite sign (that is, excitatory and inhibitory) from functionally distinct compartments. **e**, DANs (for example, DAN-g1 and DAN-i1) receive convergent inputs of opposite sign from functionally distinct compartments via distinct one-step FBN pathways. ChAT, choline acetyltransferase; GluT, vesicular glutamate transporter.

In contrast, we found that activating MBON-m1 evoked excitatory responses in DAN-i1 in three of three animals with a similar latency (47 ± 9 ms) to the inhibitory responses evoked by MBON-i1 activation (Fig. 4e–g and Supplementary Fig. 3d).

In summary, we confirmed with physiological recording an inference we had made from structural connectivity and neurotransmitter information (Fig. 3e): functionally inhibitory and excitatory MBON connections from compartments of opposite valence converge onto the same DAN (Fig. 4a–g).

Two-step feedback further increases intercompartment connectivity. We also analyzed the connections between all MBONs to all modulatory neurons via two-step pathways (Figs. 2a–c and 5a–e; Extended Data Fig. 4a–c; Supplementary Figs. 4, 5a–d and 6; Supplementary Adjacency Matrix 1 and Supplementary Atlas). We found two-step feedback pathways from most MBONs to most modulatory neurons that further increase intercompartment connectivity (Fig. 5e and Extended Data Fig. 8b). We were able to determine neurotransmitter profiles for seven neurons that provide

two-step feedback: three were cholinergic, two were GABAergic and two were glutamatergic (Fig. 5b,d and Extended Data Fig. 9). In summary, we found a diverse set of two-step feedback motifs that could support within- and cross-compartment computations.

Feedback neurons can drive memory formation. So far, we have shown that some indirect feedback connections from MBONs to DANs are functional (Fig. 4b–g). We also wanted to test whether the feedback neurons can sufficiently influence DAN activity to induce learning. We generated Split-GAL4 lines that drive expression selectively in one or very few neuron types for a cholinergic FB2N, a glutamatergic FB2N and a GABAergic FBN (Extended Data Figs. 1, 9 and 10). These neurons project onto DANs whose activation can induce aversive memory for paired odors (Fig. 1c and Extended Data Fig. 2). We asked whether optogenetic activation of these neurons is sufficient to induce memory in our olfactory training paradigm (Fig. 6). We found that activation of the excitatory cholinergic FB2N induces aversive memory for paired odors (Fig. 6a and Extended Data Fig. 2), similar to activation of its postsynaptic

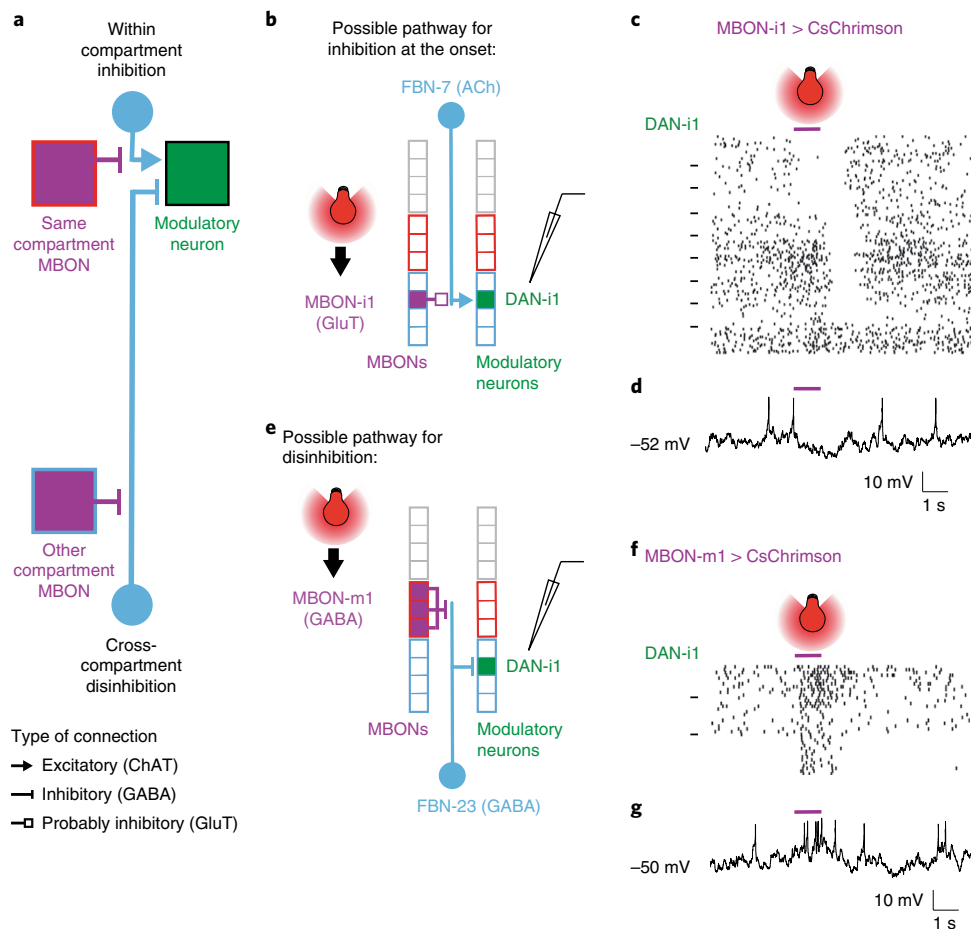


Fig. 4 | Functional inhibitory and excitatory feedback from compartments of opposite valence converge onto a DAN. **a**, Schematic diagram showing potentially inhibitory within-compartment and disinhibitory cross-compartment feedback converging onto a DAN. These two predicted connections are tested separately (**b–d** and **e–g**). **b**, The cholinergic FBN-7 downstream of the glutamatergic MBON-i1 could mediate inhibitory one-step within-compartment feedback onto DAN-i1. **c**, Whole-cell patch-clamp recording of DAN-i1 reveals inhibitory within-compartment feedback connection from MBON-i1 (purple bar). Action potentials from 180 traces from nine animals are shown as raster plots. Dashes on the left separate distinct animals. We observed long-latency inhibitory responses in DAN-i1 at the onset (top 3 of 9 animals, 55.3 ± 17.3 ms, mean \pm s.d.) or offset (next 5 of 9 animals, 95.3 ± 43.5 ms) of MBON-i1 activation (purple bar). **d**, Example trace from **c** (more in Supplementary Fig. 3a). **e**, The GABAergic FBN-23 downstream of the GABAergic MBON-m1 could mediate disinhibitory cross-compartment one-step feedback onto DAN-i1. **f**, Whole-cell patch-clamp recording of DAN-i1 reveals a functionally excitatory cross-compartment connection from MBON-m1. Action potentials from 30 traces from three animals are shown as raster plots. We observed a long-latency excitatory response in DAN-i1 at the onset of MBON-m1 activation (purple bar, 3 of 3 animals, 51.3 ± 7.7 ms). **g**, Example trace from **f** (see more details in Supplementary Fig. 3d).

DAN-f1 (Fig. 1c). Interestingly, pairing of an odor with the activation of the GABAergic FBN or the glutamatergic FB2N induces appetitive memory for paired odors (Fig. 6b,c and Extended Data Fig. 2a,b), opposite to activation of their postsynaptic DANs (Fig. 1c).

Connectivity-constrained model of the circuit reveals feedback neurons improve performance on complex learning tasks. To explore the computational consequences of the feedback neurons, we developed a model of the circuit constrained by: (1) the connectome, (2) the known neurotransmitter identities and (3) the valences of compartments (Fig. 1c). The presence or absence of connections between MBONs, DANs and feedback neurons in the model was determined by the connectome, and for neurons known to be excitatory or inhibitory, the signs of the connections were fixed to be consistent with this designation. We additionally used synapse counts from the connectome to set the initial strengths of model connections. Because synapse counts alone are unlikely to fully determine functional interactions, we then adjusted these connection strengths using gradient descent to optimize the network to

perform a set of associative learning tasks³¹ (see Methods). Unlike in standard recurrent neural network models, we modeled ongoing modifications of KC-to-MBON connections using a synaptic plasticity rule that depends on the timing of KC and modulatory neuron activity consistent with experimental findings^{16,22}.

We assessed the contributions of different feedback pathways by repeating the optimization procedure for networks lacking such feedback and by comparing their performance. Tasks included first-order conditioning and extinction that have been demonstrated in both larval^{15,32} and adult *Drosophila*^{3,33}, and second-order and context-dependent conditioning that have so far been found only in adults^{34,35}. In second-order conditioning, a reinforcement predicting CS is used to reinforce a second stimulus, whereas in context-dependent conditioning, the US valence depends on a previous contextual input.

We found that the performance on all tasks was considerably degraded in the absence of all feedback, including direct MBON feedback, one-step feedback via FBNs and two-step feedback via FB2Ns and FBNs (Fig. 7a,b). The removal of the indirect feedback

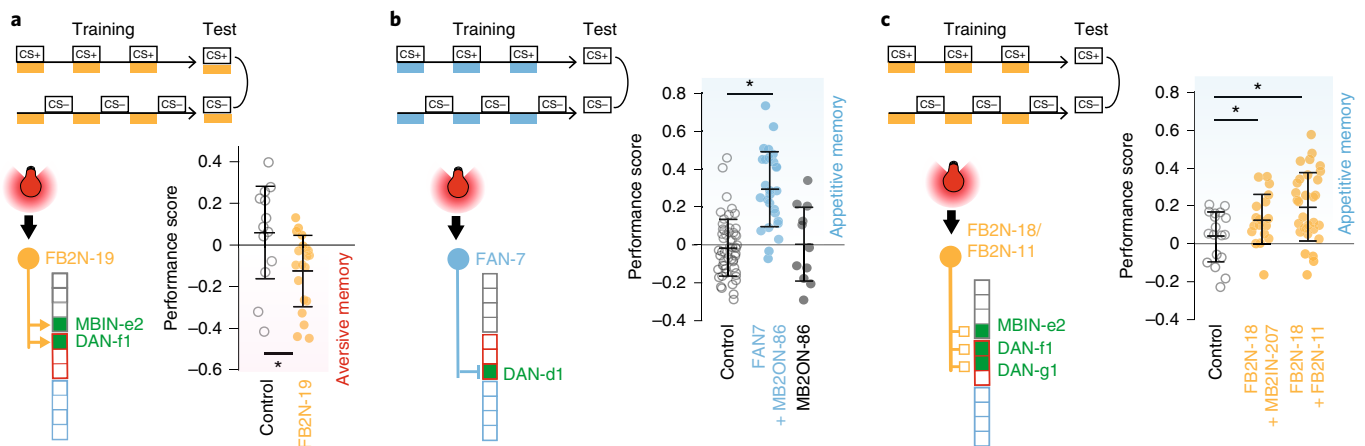


Fig. 6 | Feedback neurons can drive associative memory formation. **a–c**, We generated Split-GAL4 lines to target CsChrimson expression almost exclusively to single FBNs or FB2Ns that innervate vertical lobe DANs (see Extended Data Fig. 10). We optogenetically activated these neurons instead of a US in our associative memory paradigm (as in Fig. 1b,c). Horizontal lines indicate means and standard deviations. Statistics are as in Fig. 1c; $*P < 0.05$, two-sided Mann-Whitney U test with Holm-Bonferroni correction. **a**, Activation of the excitatory FB2N-19 in the training paradigm induces aversive memory, same as the activation of its postsynaptic DAN-f1 (Fig. 1c). $n = 13$ and 20. **b**, Activation of FAN-7 induces appetitive memory, opposite to its postsynaptic DAN-d1 (Fig. 1c). The *SS02108-Split-GAL4* line drives expression in two brain neurons, the GABAergic FAN-7 and MB2ON-86, and in a few somatosensory interneurons in the nerve cord (unlikely to evoke an appetitive memory). We therefore used the *SS04330-Split-GAL4* line that drives expression specifically in MB2ON-86 as an additional control and found this neuron did not induce memory formation. $n = 52$, 27 and 11. **c**, Activation of FB2N-18 with or without FB2N-11 induces appetitive memory, opposite to activation of their presynaptic DANs (Fig. 1c). The *SS01778-Split-GAL4* line drives expression in the glutamatergic FB2N-18 and FB2N-11, which have very similar morphology and connectivity (Supplementary Figs. 3 and 4b–d and Extended Data Fig. 10). Both connect most strongly to DAN-f1 and weakly to MBIN-e2 (and to DAN-g1 for FB2N-18). The *SS02181-Split-GAL4* line drives expression in FB2N-18 and in MB2IN-207, a weakly connected premodulatory neuron (unlikely to be able to notably influence modulatory neuron activity). $n = 18$, 18, and 31.

cross-compartment MBON-to-DAN connections have been implicated in extinction^{3,33}, but the role of indirect feedback pathways has not been investigated. In our model we find that removing indirect feedback considerably reduces performance of networks optimized to extinguish a previous association (Fig. 7a). Some modulatory neurons also showed prolonged inhibition in response to the omission of a predicted US whose valence is the same as the neuron's preferred US (Fig. 7e, fourth row). Such responses potentially represent negative prediction errors¹ and have been proposed to support extinction by erasing the memory formed by the activation of that modulatory neuron². Thus, our model raises the possibility that extinction could be implemented via multiple mechanisms in this circuit².

Discussion

Modulatory neurons (for example, DANs) are key components of higher-order circuits for adaptive behavioral control, and they provide teaching signals that drive memory formation and updating^{1,3,4,9,15,33,37}. Here, we provide a synaptic-resolution connectivity map of a recurrent neural network that regulates the activity of modulatory neurons in a higher-order learning center, the *Drosophila* larval MB (Fig. 2a–f). We also functionally tested some of the recently identified structural pathways and developed a model of the circuit to explore the roles of these motifs in different learning tasks (Fig. 7a–e).

Feedback pathways enable adaptive regulation of learning by prior learning. We discovered a large population of 61 feedback neuron pairs that provide one- and/or two-step feedback from the MBONs to modulatory neurons (Figs. 2a–d, 3a,b and 5a–e). Strikingly, we found that many modulatory neurons receive more than 50% of their total dendritic input from feedback pathways (Fig. 2d). These results suggest that prior memories as represented by the pattern of MBON activity can strongly influence modulatory neuron activity.

Learning and memory systems in vertebrates⁹ and insects^{3,14,18,19} are often organized into distinct compartments implicated in forming distinct types of memories (for example, aversive and appetitive or short and long term). Interestingly, we found that the majority of the discovered feedback pathways link distinct memory systems, suggesting that the MB functions as an interconnected ensemble during learning (Figs. 3b and 5e). Thus, prior memories formed about an odor in one compartment can influence the formation and updating of distinct types of memories about that odor in other compartments.

In adult *Drosophila*, functional connections between some MBONs and DANs^{33,37–43} have been reported, and some have been shown to play a role in short-term memory formation^{37,40,44}, long-term memory consolidation^{39,42}, extinction and reconsolidation^{3,33,41}, or in synchronizing DAN ensemble activity in a context-dependent manner³⁸. In some cases, direct MBON-to-DAN connections have been demonstrated^{33,37,39,41}. Although direct connections from several MBONs onto DANs exist in the larva¹² (Extended Data Fig. 8a), we find that indirect connections via the feedback neurons account for a much larger fraction of a modulatory neuron's dendritic input than direct MBON synapses (Fig. 2d). This suggests that adaptive DAN responses may be largely driven by such indirect feedback.

Some of the one-step within-compartment feedback motifs we found are analogous to the feedback motifs so far described for the DANs in the vertebrate midbrain^{4,45–49}. Although the diversity and the inputs of striatal feedback neurons have not yet been fully explored, in the future it will be interesting to determine whether many of the striatal feedback neurons also link distinct memory systems.

Circuit motifs for computing integrated predicted value signals across aversive and appetitive memory systems. The use of internal predictions can dramatically increase the flexibility of a learning system^{1,7,8}. Our study reveals candidate circuit motifs that could compute integrated predicted value signals across appetitive

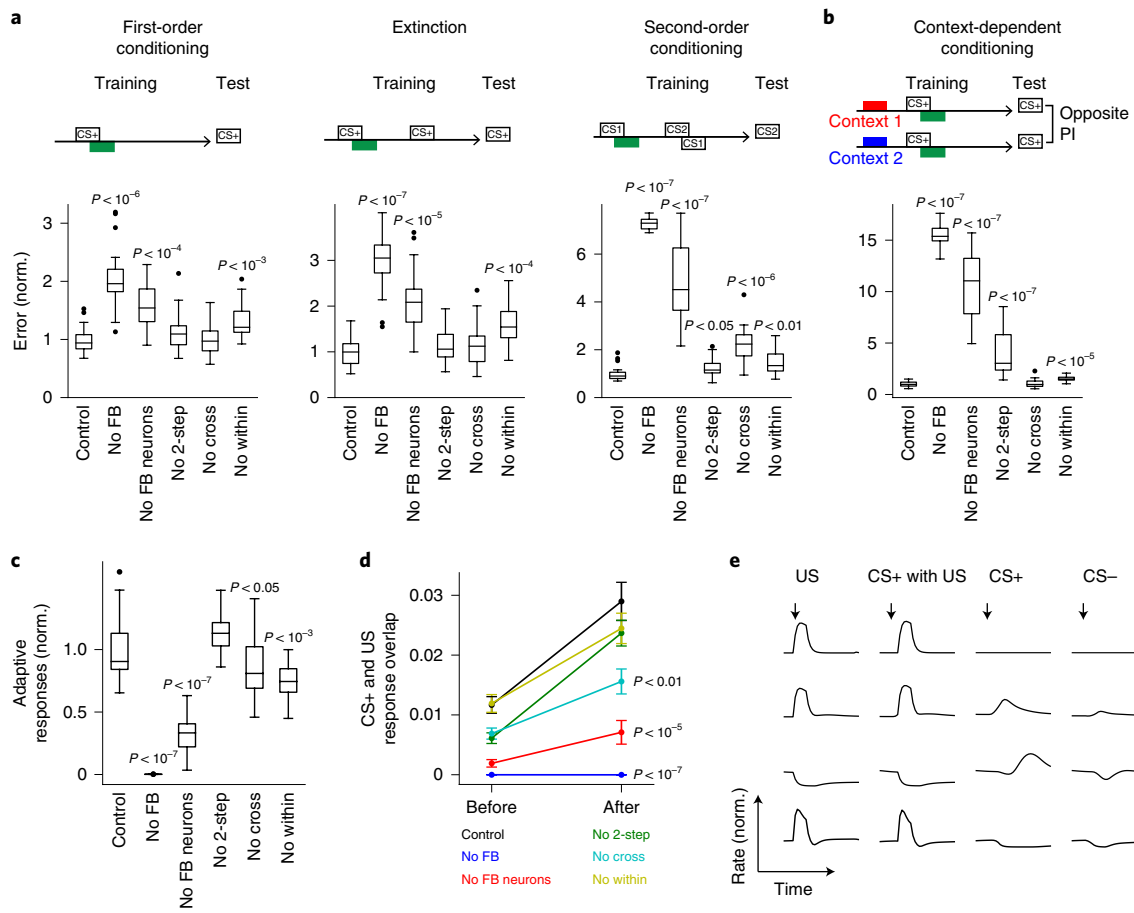


Fig. 7 | Model reveals effects of feedback motifs on learning task performance. **a**, Normalized error (mean-squared difference between decoded and target valence, normalized to error for control networks) after optimizing models to perform first-order conditioning, extinction and second-order conditioning. Error shown for six cases: control, full network; no FB, networks in which feedback onto modulatory neurons, including direct MBON connections, is removed; no FB neurons, indirect FBN/FB2N feedback is removed but direct MBON connections are intact; no two-step, only FB2Ns and all FBN-to-FBN connections are removed; no cross, indirect cross-compartment connections are removed; and no within, indirect within-compartment connections are removed. Performance of model networks was assessed by optimizing $n=20$ networks independently. Performance measures were compared across network types, and significance was assessed with a two-sided Mann-Whitney U test (**a-d**). P values represent a comparison with control networks after conditioning. Box, lower and upper quartiles; line, median; whiskers, range of the data up to 1.5x interquartile range; points outlier's of the whiskers range (**a-c**). **b**, As in **a**, but for networks optimized to perform a context-dependent conditioning task. **c**, Adaptive response index for networks in **a**, defined as the magnitude of firing rate change to CS+ presentation before and after conditioning, averaged over modulatory neurons. Results are normalized by the index for control networks. **d**, CS+ and US response overlap before and after conditioning. Overlap equals the dot product of the vectors of firing rate changes across the modulatory neuron population during CS+ and US presentations. **e**, Example responses of DANs from networks in **a** to US alone (US), CS+ paired with US following training (CS+ with US), CS+ alone after training (CS+) and CS before training (CS). First row: a DAN selective only to US. Second row: a DAN selective to US that acquires a CS+ response after conditioning. Third and fourth rows: DANs with 'prediction error'-like responses. CS+ responses are opposite in sign to US responses. Third row: a DAN inhibited by US and activated when US is omitted. Fourth row: a DAN excited by US and inhibited when US is omitted.

and aversive memory systems. A prominent motif we identified is convergence of excitatory and inhibitory connections from MBONs from compartments of opposite valence onto DANs (Figs. 3b-e and 4a-g). In naive animals, odor-evoked MBON excitation in all compartments is thought to be similar. However, associative learning selectively depresses conditioned odor drive to MBONs in compartments where modulatory neuron activation has been paired with the odor^{3,16}. We propose that by comparing the conditioned odor-evoked MBON excitation in compartments of opposite valence via cross-compartment feedback connections, modulatory neurons compute an integrated predicted value signal across appetitive and aversive domains.

Convergence of feedback and US pathways could allow the computation of prediction errors. An important aspect of reinforcement

learning theories is the idea that modulatory neurons compare predicted and actual US (to compute so-called prediction errors) and drive memory formation or extinction depending on the sign of the prediction error. Although *Drosophila* modulatory neurons have not yet been directly shown to represent prediction errors, adult and larval *Drosophila* are capable of extinction^{3,32,33}, and our study reveals candidate motifs that could support the comparison of expected and actual US. We found that modulatory neurons receive convergent input from feedback pathways from MBONs and from US pathways (Fig. 2d-f). Modulatory neurons could therefore potentially compute prediction errors by comparing inhibitory drive from the feedback pathways with the excitatory drive from the US pathways, or vice versa. Consistent with this idea, we observed in our model some DANs that are inhibited by US alone and activated by CS+ alone, or vice versa (Fig. 7e, third and fourth rows).

Our study also reveals that US pathways and feedback pathways converge at two levels: not only at the modulatory neurons themselves, but also at the FB2Ns (Fig. 2f). Actual and expected outcomes could therefore also be compared by FB2Ns. A recent study in the mouse ventral tegmental area has found that some pre-DAN neurons encoded only actual or only expected reward, whereas others encoded both variables^{4,45}. Thus, both in vertebrates and in insects, comparing predicted and actual outcomes may be a complex computation involving multiple levels of integration that eventually converge onto an ensemble of modulatory neurons⁴⁵.

Diversity of feedback inputs across modulatory neurons suggests a range of distinct and distributed teaching signals. An assumption in many reinforcement learning models is that all modulatory neurons receive a global scalar reward prediction error signal¹. Here, we were able to analyze the comprehensive set of inputs of every individual uniquely identifiable modulatory neuron in a learning center. This revealed that each modulatory neuron receives a unique set of feedback inputs (Fig. 2e) that could enable each neuron to compute a unique set of features. Consistent with this, we observed a diversity of adaptive response types in the modulatory neurons in our model (Fig. 7d). This suggests that instead of computing a single global reward prediction error that is distributed to all modulatory neurons, the network uses a range of distinct compartmentalized and distributed teaching signals.

Multilevel and cross-compartment feedback increase performance and flexibility. Our connectivity and modeling studies revealed two architectural features of the circuit that provide input to the modulatory neurons that increase its performance and flexibility on learning tasks (Fig. 7a,b). The first is the multilevel feedback architecture that includes not only the previously known direct MBON feedback^{33,37,39,41}, but also multiple levels of indirect feedback. The second is the extensive set of cross-compartment connections. Modeling suggests that these motifs support improved performance on complex tasks that require the computation of variables such as predictions, prediction errors and context.

In summary, we present a complete circuit diagram of a recurrent network that computes teaching signals in a biological system, providing insights into the architectural motifs that increase its computational power and flexibility. Our connectome-constrained model provides numerous predictions that can be tested in the future in a tractable model organism, for which genetic tools can be generated to monitor and manipulate individual neurons^{26,27,50}. The connectome, together with the functional and modeling studies, therefore provides exciting opportunities for elucidating the biological implementation of reinforcement learning algorithms.

Reporting summary

Further information on the research design is available in the Nature Research Reporting Summary linked to this article.

Online content

Any methods, additional references, Nature Research reporting summaries, source data, extended data, supplementary information, acknowledgements, peer review information; details of author contributions and competing interests; and statements of data and code availability are available at <https://doi.org/10.1038/s41593-020-0607-9>.

Received: 16 August 2019; Accepted: 6 February 2020;
Published online: 23 March 2020

References

- Schultz, W. Neuronal reward and decision signals: from theories to data. *Physiol. Rev.* **95**, 853–951 (2015).
- Dunsmoor, J. E., Niv, Y., Daw, N. & Phelps, E. A. Rethinking extinction. *Neuron* **88**, 47–63 (2015).
- Cognigni, P., Felsenberg, J. & Waddell, S. Do the right thing: neural network mechanisms of memory formation, expression and update in *Drosophila*. *Curr. Opin. Neurobiol.* **49**, 51–58 (2018).
- Watabe-Uchida, M., Eshel, N. & Uchida, N. Neural circuitry of reward prediction error. *Annu. Rev. Neurosci.* **40**, 373–394 (2017).
- Menzel, R. Searching for the memory trace in a mini-brain, the honeybee. *Learn. Mem.* **8**, 53–62 (2001).
- Heisenberg, M. Mushroom body memoir: from maps to models. *Nat. Rev. Neurosci.* **4**, 266–275 (2003).
- Rescorla, R.A. & Wagner, A.R. in *Classical Conditioning II: Current Research and Theory* (eds Black, A.H. & Prokasy, W.F.) 64–99 (Appleton Century Crofts, 1972).
- Sutton, R. S. & Barto, A. G. *Reinforcement Learning: An Introduction* (MIT Press, 1998).
- Watabe-Uchida, M. The basal ganglia sensory system listens to prefrontal task needs. *Neuron* **103**, 353–355 (2019).
- Riemensperger, T., Vller, T., Stock, P., Buchner, E. & Fiala, A. Punishment prediction by dopaminergic neurons in *Drosophila*. *Curr. Biol.* **15**, 1953–1960 (2005).
- Dylla, K. V., Raiser, G., Galizia, C. G. & Szyszka, P. Trace conditioning in *Drosophila* induces associative plasticity in mushroom body kenyon cells and dopaminergic neurons. *Front. Neural Circuits* **11**, 42 (2017).
- Eichler, K. et al. The complete connectome of a learning and memory centre in an insect brain. *Nature* **548**, 175–182 (2017).
- Takemura, S. Y. et al. A connectome of a learning and memory center in the adult *Drosophila* brain. *eLife* **6**, e26975 (2017).
- Davis, R. L. Traces of *Drosophila* memory. *Neuron* **70**, 8–19 (2011).
- Thum, A. S. & Gerber, B. Connectomics and function of a memory network: the mushroom body of larval *Drosophila*. *Curr. Opin. Neurobiol.* **54**, 146–154 (2019).
- Handler, A. et al. Distinct dopamine receptor pathways underlie the temporal sensitivity of associative learning. *Cell* **178**, 60–75.e19 (2019).
- Hige, T., Aso, Y., Modi, M. N., Rubin, G. M. & Turner, G. C. Heterosynaptic plasticity underlies aversive olfactory learning in *Drosophila*. *Neuron* **88**, 985–998 (2015).
- Waddell, S. Reinforcement signalling in *Drosophila*; dopamine does it all after all. *Curr. Opin. Neurobiol.* **23**, 324–329 (2013).
- Aso, Y. & Rubin, G. M. Dopaminergic neurons write and update memories with cell-type-specific rules. *eLife* **5**, e16135 (2016).
- Liu, C. et al. A subset of dopamine neurons signals reward for odour memory in *Drosophila*. *Nature* **488**, 512–516 (2012).
- Schroll, C. et al. Light-induced activation of distinct modulatory neurons triggers appetitive or aversive learning in *Drosophila* larvae. *Curr. Biol.* **16**, 1741–1747 (2006).
- Saumweber, T. et al. Functional architecture of reward learning in mushroom body extrinsic neurons of larval *Drosophila*. *Nat. Commun.* **9**, 1104 (2018).
- Caldwell, J. C., Miller, M. M., Wing, S., Soll, D. R. & Eberl, D. F. Dynamic analysis of larval locomotion in *Drosophila* chordotonal organ mutants. *Proc. Natl Acad. Sci. USA* **100**, 16053–16058 (2003).
- Tracey, W., Wilson, R., Laurent, G. & Benzer, S. *painless*, a *Drosophila* gene essential for nociception. *Cell* **113**, 261–273 (2003).
- Ohyama, T. et al. High-throughput analysis of stimulus-evoked behaviors in *Drosophila* larva reveals multiple modality-specific escape strategies. *PLoS One* **8**, e71706 (2013).
- Ohyama, T. et al. A multilevel multimodal circuit enhances action selection in *Drosophila*. *Nature* **520**, 633–639 (2015).
- Jovanic, T. et al. Competitive disinhibition mediates behavioral choice and sequences in *Drosophila*. *Cell* **167**, 858–870.e19 (2016).
- Eschbach, C. et al. Associative learning between odorants and mecha-nosensory punishment in larval *Drosophila*. *J. Exp. Biol.* **214**, 3897–3905 (2011).
- Liu, W. W. & Wilson, R. I. Glutamate is an inhibitory neurotransmitter in the *Drosophila* olfactory system. *Proc. Natl Acad. Sci. USA* **110**, 10294–10299 (2013).
- Fushiki, A. et al. A circuit mechanism for the propagation of waves of muscle contraction in *Drosophila*. *eLife* **5**, e13253 (2016).
- Jiang, L. & Litwin-Kumar, A. Models of heterogeneous dopamine signaling in an insect learning and memory center. Preprint at *bioRxiv* <https://doi.org/10.1101/737064> (2019).
- Mancini, N. et al. Reversal learning in *Drosophila* larvae. *Learn. Mem.* **26**, 424–435 (2019).
- Felsenberg, J. et al. Integration of parallel opposing memories underlies memory extinction. *Cell* **175**, 709–722.e15 (2018).
- Tabone, C. J. & de Belle, J. S. Second-order conditioning in *Drosophila*. *Learn. Mem.* **18**, 250–253 (2011).
- Brembs, B. & Wiener, J. Context and occasion setting in *Drosophila* visual learning. *Learn. Mem.* **13**, 618–628 (2006).

36. Schultz, W., Dayan, P. & Montague, P. R. A neural substrate of prediction and reward. *Science* **275**, 1593–1599 (1997).
37. Zhao, X., Lenek, D., Dag, U., Dickson, B. J. & Keleman, K. Persistent activity in a recurrent circuit underlies courtship memory in *Drosophila*. *eLife* **7**, e31425 (2018).
38. Cohn, R., Morante, I. & Ruta, V. Coordinated and compartmentalized neuromodulation shapes sensory processing in *Drosophila*. *Cell* **163**, 1742–1755 (2015).
39. Ichinose, T. et al. Reward signal in a recurrent circuit drives appetitive long-term memory formation. *eLife* **4**, 1–18 (2015).
40. Ueoka, Y., Hiroi, M., Abe, T. & Tabata, T. Suppression of a single pair of mushroom body output neurons in *Drosophila* triggers aversive associations. *FEBS Open Bio.* **7**, 562–576 (2017).
41. Felsenberg, J., Barnstedt, O., Cognigni, P., Lin, S. & Waddell, S. Re-evaluation of learned information in *Drosophila*. *Nature* **544**, 240–244 (2017).
42. Pavlowsky, A., Schor, J., Placais, P. Y. & Preat, T. A gabaergic feedback shapes dopaminergic input on the *Drosophila* mushroom body to promote appetitive long-term memory. *Curr. Biol.* **28**, 1783.e4–1793.e4 (2018).
43. König, C., Khalili, A., Niewalda, T., Gao, S. & Gerber, B. An optogenetic analogue of second-order reinforcement in *Drosophila*. *Biol. Lett.* **15**, 20190084 (2019).
44. Lyutova, R. et al. Reward signaling in a recurrent circuit of dopaminergic neurons and peptidergic kenyon cells. *Nat. Commun.* **10**, 3097 (2019).
45. Tian, J. et al. Distributed and mixed information in monosynaptic inputs to dopamine neurons. *Neuron* **91**, 1374–1389 (2016).
46. Beier, K. T. et al. Circuit architecture of vta dopamine neurons revealed by systematic input-output mapping. *Cell* **162**, 622–634 (2015).
47. Haber, S. N., Fudge, J. L. & McFarland, N. R. Striatonigrostriatal pathways in primates form an ascending spiral from the shell to the dorsolateral striatum. *J. Neurosci.* **20**, 2369–2382 (2000).
48. Watabe-Uchida, M., Zhu, L., Ogawa, S. K., Vamanrao, A. & Uchida, N. Whole-brain mapping of direct inputs to midbrain dopamine neurons. *Neuron* **74**, 858–873 (2012).
49. Menegas, W. et al. Dopamine neurons projecting to the posterior striatum form an anatomically distinct subclass. *eLife* **4**, e10032 (2015).
50. Pfeiffer, B. D. et al. Refinement of tools for targeted gene expression in *Drosophila*. *Genetics* **186**, 735–755 (2010).

Publisher's note Springer Nature remains neutral with regard to jurisdictional claims in published maps and institutional affiliations.

© The Author(s), under exclusive licence to Springer Nature America, Inc. 2020

Methods

Fly lines. In the main text and figures, short names are used to describe genotypes for clarity. See Supplementary Table 1 for a complete list of full names of all driver lines and effectors. We used GAL4, Split-GAL4 lines to direct the expression of the red-shifted channel-rhodopsin *20xUAS-CsChrimson-mVenus* (ref. ⁵¹; Bloomington *Drosophila* Stock Center BDSC 55134, gift of V. Jayaraman) or the calcium indicator *20xUAS-IVS-GCaMP6f* (ref. ⁵²) in pairs of neurons or subsets of neurons. Split-GAL4 lines restrict expression of the effector to a few cells, under the double control of two enhancers (inserted in the attP2 and attP40 docking sites), selected by us or others in the Janelia Research Campus (HHMI) based on their GAL4 expression pattern^{50,53,54}.

Modulatory neurons (MBINs). We used *SS24765-Split-GAL4* to optogenetically activate OAN-a1 in the calyx. We generated *SS02160-Split-GAL4* to activate DAN-c1 in the lower peduncle. For the vertical lobe, we generated *SS01702-Split-GAL4* to activate or image calcium transients in MBIN-e2 (DAN-c1 was also covered by this line) and *SS01958-Split-GAL4* to activate or image calcium transients in OAN-e1 in the upper vertical lobe (UVL). We used *SS02180-Split-GAL4*, *MB145B-Split-GAL4* (used for activation and calcium imaging, gift of G. Rubin and Y. Aso) and *MB065B-Split-GAL4* (ref. ⁵⁵) (which also covered DAN-c1) to target DAN-f1 in the intermediate vertical lobe (IVL). We used *SS01716-Split-GAL4* (ref. ²²) to induce or image DAN-g1 activity in the lower vertical lobe (LVL), and we generated *SS04268-Split-GAL4* to activate OAN-g1, also in the LVL. *MB054B-Split-GAL4* (gift of G. Rubin and Y. Aso) was also used to coactivate DAN-g1 and DAN-f1. We used two lines to target DAN-d1 in the lateral appendix: *MB143B-Split-GAL4* (used for activation and calcium imaging) and *MB328B-Split-GAL4* (both gifts of G. Rubin and Y. Aso). In the medial lobe, we generated a broad line *SS01948-GAL4*, which allows coactivation of DAN-h1, DAN-i1, DAN-k1 and sometimes DAN-j1. We also imaged calcium transients in DAN-i17 using the more specific *GAL4 SS00864-Split-GAL4*.

Neurons presynaptic to the modulatory neurons (MBINs). We optogenetically activated multidendritic class IV neurons (MD IV) with the driver line *ppk-1.9-GAL4* (gift of D. Tracey), Basin interneurons with *GMR72F11-GAL4* (ref. ²⁶) and the ascending neuron A00c with *GMR71A10-GAL4* (refs. ^{26,56}) crossed to *ppk-GAL80* (ref. ⁵⁷) and *repo-GAL80* (ref. ⁵⁸) (to prevent expression in MD IV and glial cells, respectively). We also activated A00c with the more specific GAL4 line *SS00883-Split-GAL4*. We generated *SS01778-Split-GAL4* and *SS02181-Split-GAL4*, which target FB2N-11 and/or FB2N-18. *SS02108-Split-GAL4* targets FAN-7, and *SS02401-Split-GAL4* targets FB2N-19.

Control lines. As a control for the GAL4 lines inserted at the attP2 site, we used the empty control stock *y w; attP2* (refs. ^{50,54}) crossed to the effector line. As a control for Split-GAL4 lines with an activation domain (AD) at attP40 and a DNA-binding domain (DBD) at attP2, we used the empty stock *y w; attP40; attP2* (refs. ^{50,54}) crossed to the effector line.

Lines for recording neuronal activity. Calcium transients in modulatory neurons were imaged using the following constructs to verify functional input of mechano-chordotonal neurons: *w; iav-LexA* (ref. ²⁶) in *attP40*; *20xUAS-IVS-GCaMP6f 15.693* (ref. ⁵²) in *attP2* and *13XLexAop2-CsChrimson-tdTomato* (ref. ⁵¹) in *VK00005*; for Basins multisensory interneurons: *w; GMR72F11-LexA* (ref. ⁵⁴) in *JK22C*, *20xUAS-IVS-GCaMP6f 15.693* (ref. ⁵²) at *attP2* and *13XLexAop2-CsChrimson-tdTomato* (ref. ⁵¹) at *VK00005*; and for MD class IV nociceptive neurons: *w; 13XLexAop2-CsChrimson-mVenus* (ref. ⁵¹) at *attP40* (BDSC 55138), *ppk-1kb-hs43-lexA-GAD10* at *attP2* and *20xUAS-IVS-GCaMP6f* (ref. ⁵²) at *VK00005*. All of the effectors used in these stocks are a gift from V. Jayaraman. Transvection was tested by bathing some samples in 100 mM mecaminylamine and observing the disappearance of responses to optogenetic stimulation (data not shown). If a response remained during mecaminylamine application, the experiments were repeated using a spatially defined photostimulation using spatial light modulator technology (see “Functional connectivity assays” below for details of the procedure and the lines concerned).

For patch-clamp recording, we crossed the genetic driver lines for MBON-m1 (*SS02163-Split-GAL4*) or for MBON-i1 (*SS01726-Split-GAL4*) to *58E02-LexAop65* at *attP40* (ref. ⁵⁹); *13xLexAop2-IVS-GCaMP6f-p10 15.693* (ref. ⁵²) at *VK00005* (BDSC 44276) and *20xUAS-CsChrimson-mCherry* (ref. ⁵¹) at *su(Hw)attP1* to activate MBONs and visualize the medial lobe DANs for patch clamping. Only data for DAN-i1, which was the most frequently hit by the recording pipette, as revealed by post hoc identification, are shown.

The reporter *pJFRC29-10xUAS-IVS-myr::GFP-p10* (ref. ⁶⁰) at *attP2* was used for immunostaining.

Learning experiments. Learning experiments were performed as previously described^{12,21,22}. The larvae, with CsChrimson-expressing neurons, were reared in the dark at 25°C in food vials supplemented with 1:200 retinal. The experimenter selected two groups of 30 third instar larvae and was blind to their specific genotype. The two groups underwent a training procedure involving odor and light exposures, either fully overlapping in time (paired group) or fully nonoverlapping (unpaired group). The paired group was placed for 3 min on 4% agarose plates and exposed

to constant red light illumination (wavelength: 629 nm, power: 350 μW cm⁻²; except for *ppk-1.9-GAL4*, which targets neurons at the surface of the body and for which a light power of 35 μW cm⁻² was used) paired with the presentation of 12 μl odor ethyl-acetate (10⁻⁴ dilution in distilled water) absorbed on two filter papers located on the plate lid. These larvae were then transferred to a new plate with no odor and in the dark for 3 min. This paired training cycle was repeated three times in total. The unpaired group of larvae underwent odor presentation in the dark and red light without odor following the same protocol. The order of the sequence of presentation for odor and light stimulation (that is for the paired group: half of the training protocols are in the sequence odor+/air-/odor+/air-/odor+/air- and half are air-/odor+/air-/odor+/air-/odor+, same logic for the unpaired group) was alternated throughout all experiments. After a 3-min test with odor presentation on one side of the plate lid, larvae were counted on the side of the odor, on the opposite side, and in the 1-cm-wide midline of the plate. Preference and performance indices were calculated as in a previous study⁶¹. In brief, a preference index (PI) was first computed for each group as: $PI = [n(\text{larvae on the odor side}) - n(\text{larvae on the no-odor side})] / N(\text{total})$, where $N(\text{total})$ includes larvae in the middle of the plate. Individual learning performance score (LPS) was then computed for each pair of the reciprocally trained group, as $LPS = [PI(\text{paired}) - PI(\text{unpaired})] / 2$. Positive scores indicate a larger proportion of larvae choosing the odor side in the paired group than in the unpaired group (that is, appetitive olfactory memory), whereas negative scores indicate the reverse inequality (that is, aversive olfactory memory). Because we tested larvae immediately after the last training trial, and less than 20 min after the first training trial, we assume the test reveals mainly short-term memory¹⁵. Experiments were performed en bloc for multiple genotypes with the same control line, as shown in the figures. The same genotype was tested over multiple days at random times of the day.

Circuit mapping and EM. We reconstructed neurons and annotated synapses in a single, complete CNS from a 6-h-old female [iso] *Canton S G1 × w1118 [iso]* 5905 larva, acquired with serial section transmission EM at a resolution of 3.8 × 3.8 × 50 nm³, which was first published along with the detailed sample preparation protocol²⁶. In brief, the CNS was dissected and placed in 2% glutaraldehyde 0.1 M sodium cacodylate buffer (pH 7.4). An equal volume of 2% OsO₄ was added, and the larva was fixed with a Pelco BioWave microwave oven with 350-, 375- and 400-W pulses for 30 s each, separated by 60-s pauses, and followed by another round of microwaving but with 1% OsO₄ solution in the same buffer. Next, samples were stained en bloc with 1% uranyl acetate in water and microwaved at 350 W for 3 × 3 for 30 s with 60-s pauses. Samples were dehydrated in an ethanol series, transferred to propylene oxide, and infiltrated and embedded with Epon resin. After sectioning the volume with a Leica UC6 ultramicrotome, sections were imaged semi-automatically with Legikon⁶² driving an FEI Spirit TEM (Hillsboro, OR, USA) and then assembled with TrakEM2 (ref. ⁶³) using the elastic method⁶⁴. The volume is available at <https://11em.catmaid.virtualflybrain.org/?pid=1>.

To map the wiring diagram, we used the web-based software CATMAID⁶⁵, updated with a suite of neuron skeletonization and analysis tools⁶⁶, and applied the iterative reconstruction method⁶⁶. All annotated synapses in this wiring diagram fulfill the four following criteria of mature synapses^{26,66}: (1) there is a clearly visible T-bar or ribbon on at least two adjacent z sections; (2) there are multiple vesicles immediately adjacent to the T-bar or ribbon; (3) there is a cleft between the presynaptic and the postsynaptic neurites, visible as a dark-light-dark parallel line; and (4) there are postsynaptic densities, visible as dark staining at the cytoplasmic side of the postsynaptic membrane.

We validated the reconstructions as previously described^{26,66}, a method successfully used in multiple studies^{26,27,30,66–68}. In brief, in *Drosophila*, as in other insects, the gross morphology of many neurons is stereotyped, and individual neurons are uniquely identifiable based on morphology^{68–70}. Furthermore, the nervous system in insects is largely bilaterally symmetric and homologous, with mirror-symmetric neurons reproducibly found on the left and the right side of the animal. We therefore validated neuron reconstructions by independently reconstructing synaptic partners of homologous neurons on the left and right sides of the nervous system. With this approach, we have previously estimated the false-positive rate of synaptic contact detection to be 0.0167 (1 error per 60 synaptic contacts)²¹. Assuming the false-positive rates are uncorrelated, for an n -synapse connection the probability that all n are wrong (and thus that the entire connection is a false positive) occurs at a rate of 0.0167 ^{n} . Thus, the probability that a connection is a false positive reduces dramatically with the number of synaptic contacts contributing to that connection. Even for $n = 2$ synaptic contacts, the probability that a connection is not true is 0.00028 (once in every 3,586 two-synapse connections). We therefore consider ‘reliable’ connections those for which the connections between the left and right homologous neurons have at least three synapses each and their sum is at least 10. See Ohyama et al.²⁶ and Schneider-Mizell et al.⁶⁶ for more details.

We also systematically asked what percentage of connections was conserved between left and right homologs, as a function of the number of synapses in that connection. We did this for the 426 neurons that were presynaptic to MBINs on the left or the right. Thus, we found that if two neurons were connected with 1, 2, 3, 4, 5, 6, 7, 8, 9 and 10 synapses on one hemisphere, the probability that homologous neurons are connected on the other hemisphere was 48%, 60%, 80%,

89%, 95%, 97%, 99%, 100%, 100% and 100%, respectively. We also computed the fraction of input that each MBIN received from each presynaptic neuron and found that if a presynaptic neuron accounted for 1.6%, 2%, 3%, 4% and 5% of a postsynaptic neuron's input, then the likelihood that the homologous neurons were connected on the other hemisphere was 95%, 99%, 100%, 100% and 100%, respectively. Thus, numerically weak connections were not conserved, but numerically strong connections were 100% conserved. Interestingly, in previous studies we have demonstrated that in the numerically strong connections in which the postsynaptic neuron receives at least 2% of input, the presynaptic neurons were also functional^{26,27}.

Thus, the numerically strong connections (that account for at least 2% of a postsynaptic neuron's input) are reproducible between left and right hemispheres of the same individuals and across individuals, as evidenced by our functional connectivity experiments across individuals.

Immunostaining. Dissected brains were fixed in phosphate-buffered saline (PBS; NaCl 137 mM, KCl 2.7 mM, Na₂HPO₄ 8.1 mM, KH₂PO₄ 1.5 mM, pH 7.3) containing 4% paraformaldehyde (Merck) for 30 min at room temperature. After two 15-min washes with PBT (PBS with 1% or 3% Triton X-100; Sigma-Aldrich), the brains were blocked with 5% normal goat serum (Vector Laboratories) in PBT and incubated for at least 24 h with primary antibodies at 4 °C. Before application of the secondary antibodies for at least 24 h at 4 °C or for 2 h at room temperature, brains were washed several times with PBT. After that, brains were again washed with PBT, mounted in Vectashield (Vector Laboratories) and stored at 4 °C in darkness. Images were taken with a Zeiss LSM 710M confocal microscope. The resulting image stacks were projected and analyzed with the image processing software Fiji (ref. ⁷¹). Primary antibodies were used at the following dilutions: rabbit anti-GFP (catalog no. Af2020, 1:1,000; Frontier Institute), chick anti-GFP (ab13970, 1:1,000; Abcam), rabbit anti-GABA (A2052, Sigma; 1:100) and mouse anti-ChAT (ChAT4B1, DSHB Hybridoma Product deposited by P.M. Salvaterra; 1:50). Rabbit anti-DVGlut⁷² was diluted 1:1,000. These antibodies were used in *Drosophila* larvae previously^{12,30}. Secondary antibodies were used at the following dilutions: Alexa Fluor 568-conjugated goat anti-rabbit immunoglobulin G (IgG; A-11036, 1:300; Invitrogen Molecular Probes), Alexa Fluor 633-conjugated goat anti-mouse IgG (A-21050, 1:300; Invitrogen Molecular Probes) and Alexa Fluor 488-conjugated goat anti-chicken IgG (A-11039, 1:300; Invitrogen Molecular Probes).

Identifying GAL4 lines that drive expression in modulatory neurons and their presynaptic partners. To identify GAL4 lines (listed in Supplementary Table 1) that drive expression in specific neurons, we performed single-cell FlpOut experiments (for FlpOut methodology, see Ohyama et al.²⁶ and Nern et al.⁷³) of many candidate GAL4 lines⁷⁴. We generated high-resolution confocal image stacks of individual neuron morphology (multiple examples per cell type). Most MBONs and MBINs were uniquely identifiable based on the dendritic and axonal projection patterns (which MB compartment they project to and the shape of input or output arbor outside the MB). These were also compared with previously reported single-cell FlpOuts of DANs and OANs in the larva^{26,61,75–77}. For the neurons upstream of MBINs (FBNs/FANs/FB2Ns), we used morphology and cell body position to identify the lineage of the neuron. The precise shape and three-dimensional location of dendritic and axonal projections were then examined and compared with all potential candidates in the lineage, which have been fully reconstructed from the EM volume. In some cases, two neurons had very similar morphology at both light and EM level, and in such cases they also had nearly identical connectivity (for example, FB2N-11 and FB2N-18).

Functional connectivity assays. CNSs of third instar larvae were dissected in a cold buffer containing 103 mM NaCl, 3 mM KCl, 5 mM TES, 26 mM NaHCO₃, 1 mM NaH₂PO₄, 8 mM trehalose, 10 mM glucose, 2 mM CaCl₂ and 4 mM MgCl₂ and adhered to poly-L-lysine (P1524; Sigma)-coated cover glass in small Sylgard (Dow Corning) plates.

For optogenetic activation, red illumination (617-nm High-Power Lightguide Coupled LED Source; Mightex) was positioned above the sample to depolarize the axon terminal parts of the sensory neurons (MD IV or chordotonal) or the second-order interneurons (Basins). Light stimulations were performed with 1- or 15-s duration and in 40 and 600 cycles of laser on/off pulses of 20/5 ms. Each preparation underwent three types of light stimulation of increasing power: ~390, 920 and 4.6 mW mm⁻². Only the data for the highest light power during 1 s is displayed (Fig. 1f). The same stimulus was spaced with 30 s for a total of three presentations in each scan. Each scan consisted of imaging DANs on a two-photon scanning microscope (Bruker) using a 60× 3.1.1 numerical aperture objective (Olympus). A mode-locked Ti:Sapphire laser (Chameleon Ultra II; Coherent) tuned to 925 nm was used for photoactivation of the GCaMP6f. Fluorescence was collected with photomultiplier tubes (Hamamatsu) after band-pass filtering. Images were acquired in line scanning mode (5.15 frames s⁻¹) for a single plane of the CNS. The same genotype was tested over multiple days at random times of the day. Data collection and analysis were not performed blind to the conditions of the experiments.

To overcome transvection observed between the transgenes at the attP40 landing site of the *MB143B-Split-GAL4* line (targeting DAN-d1) crossed to *w; 13XLexAop2-CsChrimson-mVenus* (ref. ⁵¹) in attP40, ppk-1kb-hs43-lexA-GAD10

in attP2 and 20xUAS-IVS-GCaMP6f2 in VK00005, we used three-dimensional spatially defined photostimulation. MD IV neurons expressing CsChrimson were photo-activated by a holographic pattern generated by a two-photon 1,040-nm laser (femtoTrain; Spectra-Physics) coupled to a phase-only spatial light modulator (Intelligent Imaging Innovations). GCaMP6f signal was imaged by a laser tuned to 925 nm (Insight DS+ Dual; Spectra-Physics). The optogenetic stimulations were 50 cycles of laser on/off pulses of 2 ms/18 ms, ranging from 1 to 1.5 mW mm⁻². Off-target (equidistant from the Chrimson-expressing DAN-d1 neuron, but not targeting Chrimson-expressing MD IV neurons) and on-target stimulations were alternatively performed, and the difference between transvection-only-generated calcium signals and transvection + MD IV neuron activation-generated signal was computed and used as the fluorescence signal. DAN-d1 neurons were imaged at a frame rate of ~5 frames s⁻¹ on a two-photon scanning microscope (Vivo; Intelligent Imaging Innovations) using a 25× 2.1.1 numerical aperture objective (Nikon).

For image analysis, image data were processed by Fiji software⁷¹ and analyzed using a custom code in Matlab (The Mathworks, Inc). Specifically, we manually determined the regions of interest from maximum intensity projection of entire time-series images and measured the mean intensity. In all cases, changes in fluorescence were calculated relative to baseline fluorescence levels (F_0) as determined by averaging over a period of at least 2 s just before the optogenetic stimulation. The $\delta F/F_0$ values were calculated as $\delta F/F_0 = (F_i - F_0)/F_0$, where F_i is the fluorescent mean value of a region of interest in a given frame. Analyses were performed on the mean $\delta F/F_0$ of the consecutive three stimulations.

Whole-cell patch-clamp recordings from DANs on optogenetic activation

of MBONs. For recording, the isolated brain attached with ventral nerve cord was dissected from third instar larvae in Baines external solution⁷⁸, which contained: 135 mM NaCl, 5 mM KCl, 2 mM CaCl₂, 4 mM MgCl₂, 5 mM 2-((2-hydroxy-1,1-bis(hydroxymethyl)ethyl)amino) ethanesulfonic acid, 5 mM N-(Tris(hydroxymethyl) methyl)-2-aminoethanesulfonic acid and 36 mM sucrose. The pH was adjusted to 7.15 with NaOH, and osmolarity was 310–320 mOsm. The preparation was viewed with a 60× 1 numerical aperture water-immersion objective equipped with an Olympus microscopy (BX51WI; Olympus). GCaMP6f-labeled DANs were visualized with a 470-nm-wavelength LED. The glial sheath above the targeted DANs was ruptured using 0.1% protease (Protease XIV; Sigma-Aldrich). Recording electrodes were pulled from thick-walled glass pipette (outer diameter, 1.5 mm; inner diameter, 0.86 mm) using P-97 puller (Sutter Instruments) and fire polished to resistances of 10–15 M Ω . The Baines intracellular solution⁷⁸ contained: 140 mM potassium gluconate, 5 mM KCl, 2 mM MgCl₂, 2 mM EGTA and 20 mM HEPES. The pH was adjusted to 7.4 with KOH, and the osmolarity was 280 mOsm. Biocytin was dissolved in intracellular solution at 0.5% for further post hoc morphological identification of recorded DANs. The data were acquired and processed using Digidata 1550, Multiclamp 700B and Clampex 10.4 software (Molecular Devices). The recording was sampled at 20 kHz and filtered at 6 kHz under current-clamp mode. CsChrimson was activated by 617-nm-wavelength light-emitting diode.

For DAN identification, after the electrophysiology recording, the preparation containing the ventral nerve cord and brain was fixed in 4% paraformaldehyde in 0.1 M PBS overnight at 4 °C and then transferred to PBS until staining. After rinsing in PBS, the CNS preparations were placed in Streptavidin Alexa Fluor 647 (1:200) in PBS with 10% Triton X (overnight, room temperature). After rinsing, the preparations were dehydrated and mounted with dibutylphthalate polystyrene xylene (DPX). The confocal images were captured with Zeiss 800 confocal laser microscope. Alexa Fluor 647 was excited with 633-nm-wavelength light, and mCherry-tagged CsChrimson neurons were excited with 567-nm-wavelength light.

Statistics. Because most fluorescence and behavioral data were nonnormally distributed (according to a Shapiro–Wilk test), we opted for nonparametric tests for paired comparisons. Similarly, for the model, we used a nonparametric test to compare performance. No statistical methods were used to predetermine sample sizes, but the sample sizes are similar to those reported in previous publications^{22,27,41}.

For behavioral experiments, the performance scores obtained for each line tested in optogenetic reinforcement were compared with the ones of its corresponding empty line (that is, $w; attP2$ or $w; attP40; attP2$ for GAL4 or Split-GAL4, respectively) using a nonparametric Mann–Whitney U test for independent sets of data. For multiple comparisons, the probability values were compared with a threshold of 0.05 adjusted with a Holm–Bonferroni correction to balance for type I and type II statistical errors, unless otherwise stated. Across GAL4 lines, comparisons of performance scores were done using the same methodology. Data were plotted using the Matlab script `errorbarjitter`, available at <http://www.mathworks.com/matlabcentral/fileexchange/33658-errorbarjitter>.

Fluorescence analyses were done using a nonparametric Wilcoxon test for paired comparisons between the maximum $\delta F/F_0$ plus one standard deviation during 1 s before photostimulation onset and the maximum $\delta F/F_0$ at two time windows: during the 1 s of the stimulation and from 1 to 3 s after its onset.

For the clustering analysis, we looked for clusters among FBNs/FANs based on the similarity of their synaptic partners separately for input and output. To find clusters based on synaptic inputs, we defined the similarity between a pair of FBN/FANs as the cosine similarity of the vector of inputs they receive from

MBONs, where the weight of a given connection is measured as the fraction of total input synapses on the postsynaptic neuron. Specifically, for v_i and v_j being the input vectors for FBN/FANs i and j , the similarity between them is defined as: $S_{ij} = \frac{v_i \cdot v_j}{\|v_i\| \|v_j\|}$. Hierarchical clustering on the similarity matrix was done with Scipy using average linkage. We chose the top five clusters to highlight, which included all clearly differentiated groups of FBN/FANs. Clustering on the output patterns was done identically using the vectors of connectivity from FBN/FANs onto MBINs.

For the input-clustered groups, we assessed the similarity of the patterns of synaptic outputs and vice versa for the synaptic input patterns for output-clustered groups. We measured the overall group similarity as the median of all unique pairwise cosine similarities between neurons within the group. We used a permutation test to assess the significance of the observed similarities by randomizing the relationship between input pattern and output pattern for each FAN/FBN. For example, for each input-clustered group of size n , we randomly chose n output patterns and computed their median output similarity in the same way. A one-sided P value was computed from the distribution of 10,000 random permutations with a Holm–Sidak correction for multiple comparisons across the groups.

Rate model of the MBON-i1-FBN-7-DAN-i1 one-step feedback motif. To illustrate the potential effects of different FBN-baselines, we modeled the isolated MBON-i1-FBN-7-DAN-i1 feedback motif shown in Fig. 4b with rate equations, where the output of neuron type (MBON, FBN, DAN) changed over time according to the equation:

$$\tau_i \frac{dr_i}{dt} = -r_i + f\left(\sum_j w_{ij} r_j + I_i^{\text{tonic}}\right) + I_i^{\text{stim}}$$

where $f(x) = \frac{x}{1 + e^{-k(x-x_0)}}$, W is a matrix with positive and negative values corresponding to the direct interactions between neurons as shown in the circuit schematic of Fig. 4b, I_i^{tonic} is a nonnegative tonic input into neuron i , I_i^{stim} is a stimulus input provided only to MBON, τ_i is a time constant and parameters s , k and x_0 set the shape of the sigmoidal response. Equations were solved using ode45 in Matlab (The Mathworks, Inc.; see Supplementary Fig. 3).

Connectivity-constrained model of the entire MB with the feedback neurons.

Model dynamics. We constructed a recurrent network model of the larval MB containing MBONs, DANs and other feedback neurons. The network receives input from 70 KCs and external cues, such as US. The normalized firing rate r_i of neurons i is modeled as a threshold-linear function of its input:

$$\frac{dr_i}{dt} = -r_i(t) + g\left(\sum_j W_{ij} r_j(t) + b_i + I_i(t)\right) \quad (1)$$

where g represents positive rectification. Time is modeled in units of effective time constant (representing combined synaptic and membrane timescales). The connectivity matrix W_{ij} is constrained using the EM reconstruction. The vector b_i represents the static bias input to each neuron that determines its excitability, whereas $I_i(t)$ represents time-varying external input. For MBONs, this includes external input from KCs, $I_i(t) = \sum_k W_{ik}^{KC} r_k^{KC}$.

KCs are initially silent, but during the presentation of an odor CS, the activity of a random fraction f of KCs is set to 1, leading to MBON activation. We assume all-to-all KC-to-MBON connectivity. At the beginning of each trial, weights W^{KC} are initially set equal to their maximum value of $1/(N_{KC}f)$ but are modified on each timestep according to a DAN-dependent synaptic plasticity rule. A weight $W(t)$ from KC k to an MBON in compartment i evolves according to:

$$\frac{dw}{dt} = -\bar{r}_k d_i + r_k \bar{d}_i \quad (2)$$

$$\tau_w \frac{dW}{dt} = w(t) - W(t) \quad (3)$$

where d_i represents the level of dopamine in the compartment (a weighted sum of DAN inputs according to the DAN-to-MBON connectivity matrix), and r_k represents the firing rate of the KC (note that modifications of weights onto MBONs depend only on KC and DAN activity). The terms \bar{r}_k and \bar{d}_i represent the firing rate r_k and dopamine level d_i , respectively, low-pass filtered with time constant τ , which leads to an anti-Hebbian timing-dependent synaptic weight update in equation (2). Equation (3) results in $W(t)$ following these updates with a time constant of τ_w . For simplicity, we assume that all modulatory neurons induce plasticity according to this rule.

Given the model dynamics described earlier, we use gradient descent optimization to find a set of network parameters that lead to good performance on the tasks we consider. After this optimization, KC-to-MBON weights are still time-varying quantities that evolve according to equation (3), but all other parameters are fixed. Weights among DANs, MBONs and feedback neurons are constrained by the EM reconstruction. Weight matrices are initialized using

synapse counts from the EM data, scaled so that the ℓ_2 norm of the inputs received by each neuron $\sum_j W_{ij}^2 = 1.5$. Only reliable connections, as defined previously, are included. Weights from neurons known to communicate using an inhibitory neurotransmitter are then multiplied by -1 . As optimization progresses, weights from neurons of known neurotransmitter identities are constrained to maintain a consistent sign by clipping at 0. Weights that were initialized to nonzero values rarely decayed to zero during optimization ($7 \pm 1\%$ of weights, using a cutoff of 10% of each weight's initial value to determine whether it has decayed). At the beginning of a trial, MBON rates are initialized to 0, whereas DAN and feedback neuron rates are initialized to 0.1. This promotes networks in which MBONs are primarily odor driven, but some DANs and feedback neurons exhibit baseline levels of activity.

Tasks. Neuron i 's external input $I_i(t)$ represents either KC input in the case of MBONs (as described earlier), or US or contextual signals (depending on the task) in the case of DANs and FB neurons. We assume that $I_i(t) = W_i^E e_i(t)$, where W^E is initialized as a random standard Gaussian variable and $e_i(t) = 0$ or 1 depending on whether signal j is active. For most tasks, there are two signals (positive or negative US).

A linear readout of the MBONs determines the valence of the currently presented odor via $v(t) = \sum_{i \in \text{MBON}} W_i^M r_i$, where W^M is initialized as a random Gaussian variable with variance $1/N_{\text{MBON}}$. Entries of W^M corresponding to MBONs whose activation is known to produce approach or avoidance are constrained to be consistent with this sign.

Trials consist of 80 time units. In a first-order conditioning trial, a CS+ is presented for 3 time units starting randomly between $t = 5$ and $t = 15$, followed by a positive or negative US with a delay of 2 time units. A test CS+ presentation occurs between $t = 65$ and $t = 75$, and the system must output the appropriate valence of +1 or -1 depending on the US valence during this second presentation. For extinction, an additional CS+ presentation occurs randomly between $t = 35$ and $t = 45$, and the magnitude of the valence is halved for the final test CS+ presentation. For second-order conditioning, a new CS2 is presented at this time, followed by the original CS+, and the test occurs for CS2. Finally, for context-dependent conditioning, a contextual signal that determines the US valence is presented 3 time units before the first CS. At $t = 30$ and $t = 60$, firing rates are reset to their initial conditions to model an arbitrary time delay between CS presentations and preventing networks from using persistent activity, rather than synaptic plasticity, to maintain associations.

For networks trained on first-order conditioning, second-order conditioning and extinction, training consists of random second-order conditioning and extinction trials (for which first-order conditioning is a subcomponent). On each trial, there is a 50% probability that one of the signals (for example, the US) will be omitted, or a CS- odor will replace a CS+ odor, and the network will report a valence of 0 in these cases, ensuring that only valid CS-US contingencies are learned.

Optimization. The weights of the network W , the external and readout weights W^E , W^M and the biases b are optimized using PyTorch using the RMSprop optimizer (<https://pytorch.org/>). Optimization proceeds over 1,500 epochs, each of which consists of a batch of 30 trials that are used to evaluate the loss function that is minimized through gradient descent. The loss is equal to the squared distance between the actual and target valence summed over timesteps, plus a regularization term for DAN activity. The regularization term equals $\sum_{i \in \text{DAN}} [r_i(t) - 0.1]_+^2$, which penalizes DAN activity that exceeds a baseline level of 0.1. This suppresses task-unrelated DAN activity and produces more realistic activity patterns in the DANs, but our results do not qualitatively change if this regularization is removed. We used a timestep of $\Delta t = 0.5$, although we verified that our qualitative results hold for smaller timesteps.

Parameter	Notation	Value
KC coding level	f	0.1
Maximum KC-to-MBON synaptic weight	w_{\max}	$1/(N_{KC}f)$
Timing-dependent plasticity window	τ	5
Timescale of weight modifications	τ_w	5
Initial MBON rate	m_0	0
Initial DAN rate	d_0	0.1
Initial FB neuron rate	x_0	0.1
CS-US presentation length	T_{stim}	3
CS-US delay	ΔT_{US}	2
Trial length	T	80
Timestep	Δt	0.5
RMSprop learning rate	η	0.002
Batch size	B	30
Number of epochs	n_{epochs}	1,500

Data availability

The source data and statistics for Fig. 1 are available in Source Data Fig. 1. The EM volume of the whole CNS²⁶ and the reconstructed neurons and synapses included in this paper are publicly available at <https://11em.catmaid.virtuallyflybrain.org/>, accessible online thanks to the software CATMAID^{65,66}, the same software used to reconstruct and analyze the neuronal circuits included here. Supplementary Adjacency Matrices 1, 2 and 3 contain all the connectivity information for all neurons on the extended MB network discussed in the study. The light microscopy image stacks of genetic driver lines are available from the corresponding authors upon reasonable request.

Code availability

Python code (used for the model in Fig. 7) and Matlab code (used for Supplementary Fig. 3b) can be found in Supplementary Software. The Matlab code for the analysis of imaging and behavioral data is available from the corresponding author upon reasonable request.

References

51. Klapoetke, N. C. et al. Independent optical excitation of distinct neural populations. *Nat. Methods* **11**, 338–346 (2014).
52. Chen, T. W. et al. Ultrasensitive fluorescent proteins for imaging neuronal activity. *Nature* **499**, 295–300 (2013).
53. Luan, H., Peabody, N. C., Vinson, C. R. & White, B. H. Refined spatial manipulation of neuronal function by combinatorial restriction of transgene expression. *Neuron* **52**, 425–436 (2006).
54. Jenett, A. et al. A GAL4-driver line resource for *Drosophila* neurobiology. *Cell Rep.* **2**, 991–1001 (2012).
55. Aso, Y. et al. The neuronal architecture of the mushroom body provides a logic for associative learning. *eLife* **3**, e04577 (2014).
56. Vogelstein, J. T. et al. Discovery of brainwide neural-behavioral maps via multiscale unsupervised structure learning. *Science* **344**, 386–392 (2014).
57. Yang, C. H. et al. Control of the postmating behavioral switch in *Drosophila* females by internal sensory neurons. *Neuron* **61**, 519–526 (2009).
58. Awasaki, T., Huang, Y., O'Connor, M. B. & Lee, T. Glia instruct developmental neuronal remodeling through tgf-beta signaling. *Nat. Neurosci.* **14**, 821–823 (2011).
59. Liu, C. et al. A subset of dopamine neurons signals reward for odour memory in *Drosophila*. *Nature* **488**, 512–516 (2012).
60. Pfeiffer, B. D., Truman, J. W. & Rubin, G. M. Using translational enhancers to increase transgene expression in *Drosophila*. *Proc. Natl Acad. Sci. USA* **109**, 6626–6631 (2012).
61. Rohwedder, A. et al. Four individually identified paired dopamine neurons signal reward in larval *Drosophila*. *Curr. Biol.* **26**, 661–669 (2016).
62. Suloway, C. et al. Automated molecular microscopy: the new leginon system. *J. Struct. Biol.* **151**, 41–60 (2005).
63. Cardona, A. et al. Trakem2 software for neural circuit reconstruction. *PLoS ONE* **7**, e38011 (2012).
64. Saalfeld, S., Fetter, R., Cardona, A. & Tomancak, P. Elastic volume reconstruction from series of ultra-thin microscopy sections. *Nat. Methods* **9**, 717–720 (2012).
65. Saalfeld, S., Cardona, A., Hartenstein, V. & Tomancak, P. CATMAID: collaborative annotation toolkit for massive amounts of image data. *Bioinformatics* **25**, 1984–1986 (2009).
66. Schneider-Mizell, C. M. et al. Quantitative neuroanatomy for connectomics in *Drosophila*. *eLife* **5**, e12059 (2016).
67. Berck, M. E. et al. The wiring diagram of a glomerular olfactory system. *eLife* **5**, e14859 (2016).
68. Goodman, C. S., Bate, M. & Spitzer, N. C. Embryonic development of identified neurons: origin and transformation of the h cell. *J. Neurosci.* **1**, 94–102 (1981).
69. Bate, M., Goodman, C. S. & Spitzer, N. C. Embryonic development of identified neurons: segment-specific differences in the h cell homologues. *J. Neurosci.* **1**, 103–106 (1981).
70. Costa, M., Manton, J. D., Ostrovsky, A. D., Prohaska, S. & Jefferis, G. S. NBLAST: rapid, sensitive comparison of neuronal structure and construction of neuron family databases. *Neuron* **91**, 293–311 (2016).
71. Schindelin, J. et al. Fiji: an open-source platform for biological-image analysis. *Nat. Methods* **9**, 676–682 (2012).
72. Daniels, R. W., Gelfand, M. V., Collins, C. A. & DiAntonio, A. Visualizing glutamatergic cell bodies and synapses in *drosophila* larval and adult CNS. *J. Comp. Neurol.* **508**, 131–152 (2008).
73. Nern, A., Pfeiffer, B. D. & Rubin, G. M. Optimized tools for multicolor stochastic labeling reveal diverse stereotyped cell arrangements in the fly visual system. *Proc. Natl Acad. Sci. USA* **112**, E2967–E2976 (2015).
74. Li, H. H. et al. A GAL4 driver resource for developmental and behavioral studies on the larval CNS of *Drosophila*. *Cell Rep.* **8**, 897–908 (2014).
75. Selcho, M., Pauls, D., Han, K. A., Stocker, R. F. & Thum, A. S. The role of dopamine in *Drosophila* larval classical olfactory conditioning. *PLoS ONE* **4**, e5897 (2009).
76. Selcho, M., Pauls, D., Huser, A., Stocker, R. F. & Thum, A. S. Characterization of the octopaminergic and tyraminerbic neurons in the central brain of *Drosophila* larvae. *J. Comp. Neurol.* **522**, 3485–3500 (2014).
77. Pauls, D., Selcho, M., Gendre, N., Stocker, R. F. & Thum, A. S. *Drosophila* larvae establish appetitive olfactory memories via mushroom body neurons of embryonic origin. *J. Neurosci.* **30**, 10655–10666 (2010).
78. Marley, R. & Baines, R.A. Dissection of third-instar *Drosophila* larvae for electrophysiological recording from neurons. *Cold Spring Harb. Protoc.* **2011**, pdb.prot065656 (2011).

Acknowledgements

Michael Winding, Mei Shao and Casey Schneider-Mizell contributed equally to this work. We thank Fly Light at HHMI Janelia Research Campus (JRC) for generating confocal images of the GAL4 lines, J. Simpson for sharing a two-photon microscope, Y. Aso and G. Rubin for sharing unpublished driver lines, V. Jayaraman for sharing unpublished versions of CsChrimson and GCamp6f, L. Feng and I. Andrade for help with circuit mapping from EM, K. Hibbard and JRC FLY Core for generating some of the fly stocks, Fly EM at JRC for generating the EM volume, T. Saumweber for discussions, D. Bonnelly for help with analyses and Z. Zavala-Ruiz and the JRC Visiting Scientist Program and HHMI JRC for funding. M.Z. was also supported by the European Research Council Consolidator Grant 819650 - LeaRNN, by the Wellcome Trust International Recruitment Supplement 205050/A/16/Z and by the Wellcome Trust Investigator Award 205050/Z/16/Z. C.E. was also supported by the European Research Council Consolidator Grant 819650 - LeaRNN and the Wellcome Trust International Recruitment Supplement 205050/A/16/Z. A.C. was supported by Wellcome Trust Grant 205038/Z/16/Z and Wellcome Trust International Recruitment Supplement 205038/A/16/Z. M.W. was also supported by the Wellcome Trust International Recruitment Supplement 205050/A/16/Z and the Wellcome Trust Investigator Award 205050/Z/16/Z. A.L.-K. was supported by the Burroughs Wellcome Foundation, the Gatsby Charitable Foundation, the Simons Collaboration on the Global Brain and NSF award DBI-1707398. B.G. received grant support from the Deutsche Forschungsgemeinschaft (Grant Nos. Ge1091/4-1 and FOR 2705-TP2). A.S.T. received grant support from the Deutsche Forschungsgemeinschaft (Grant Nos. TH1584/6-1 and TH1584/7-1).

Author contributions

C.E. conceived the study, designed and performed experiments and data analysis, and wrote the manuscript. A.F. performed circuit reconstruction and analysis, designed and performed experiments and data analysis, and wrote the manuscript. M.Z. and A.C. conceived the study, performed data analysis, and wrote the manuscript. A.L.-K. developed the model and wrote the manuscript. M.W., C.M.S.-M. and J.V.-A. performed circuit reconstruction and analysis. M.S. performed patch-clamp recordings. R.A., K.E. and T.O. performed experiments. A.S.T. and B.G. contributed data analysis, experimental design and revision of the manuscript. R.D.F. and J.W.T. contributed data and reagents.

Competing interests

The authors declare no competing interests.

Additional information

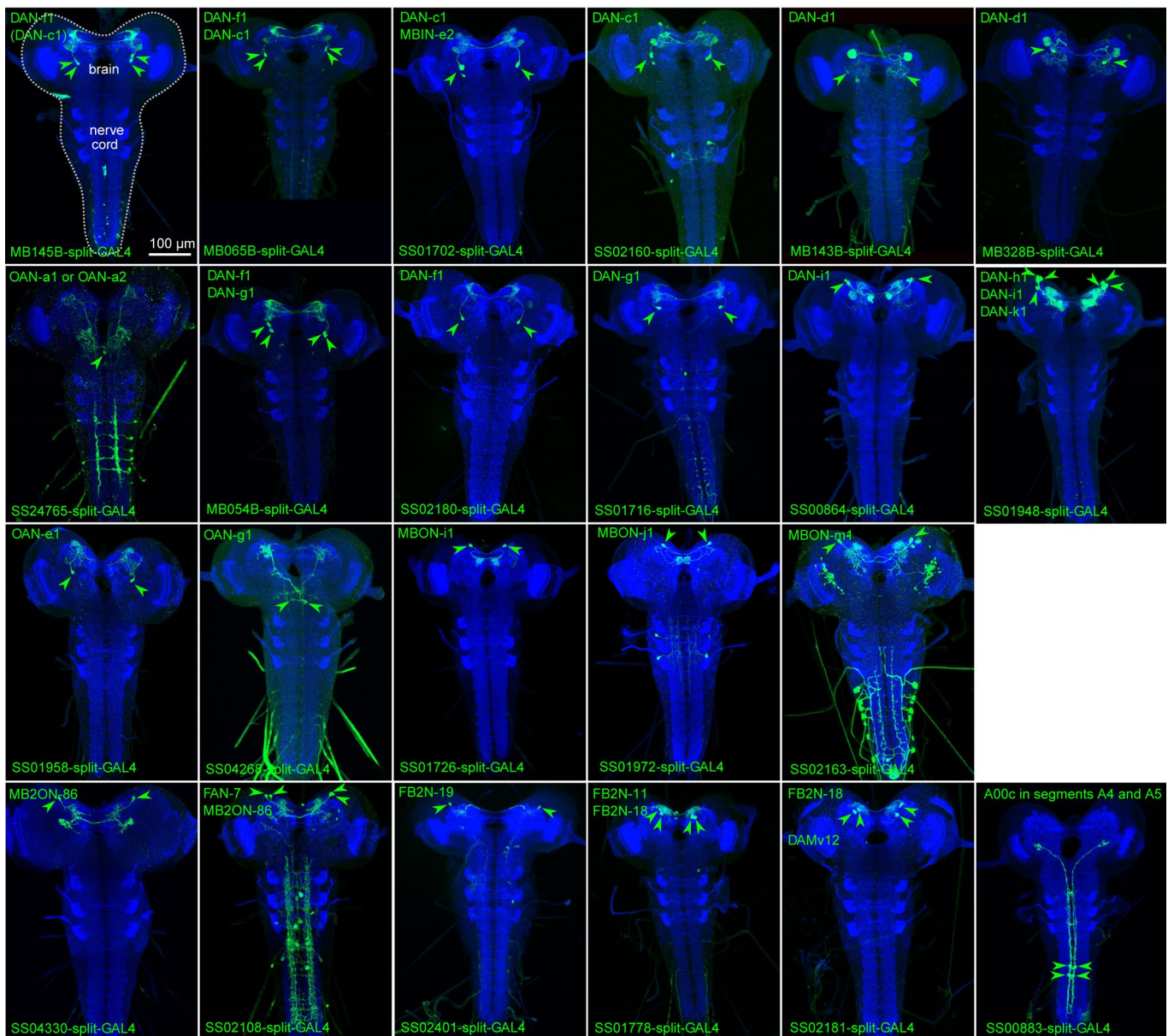
Extended data is available for this paper at <https://doi.org/10.1038/s41593-020-0607-9>.

Supplementary information is available for this paper at <https://doi.org/10.1038/s41593-020-0607-9>.

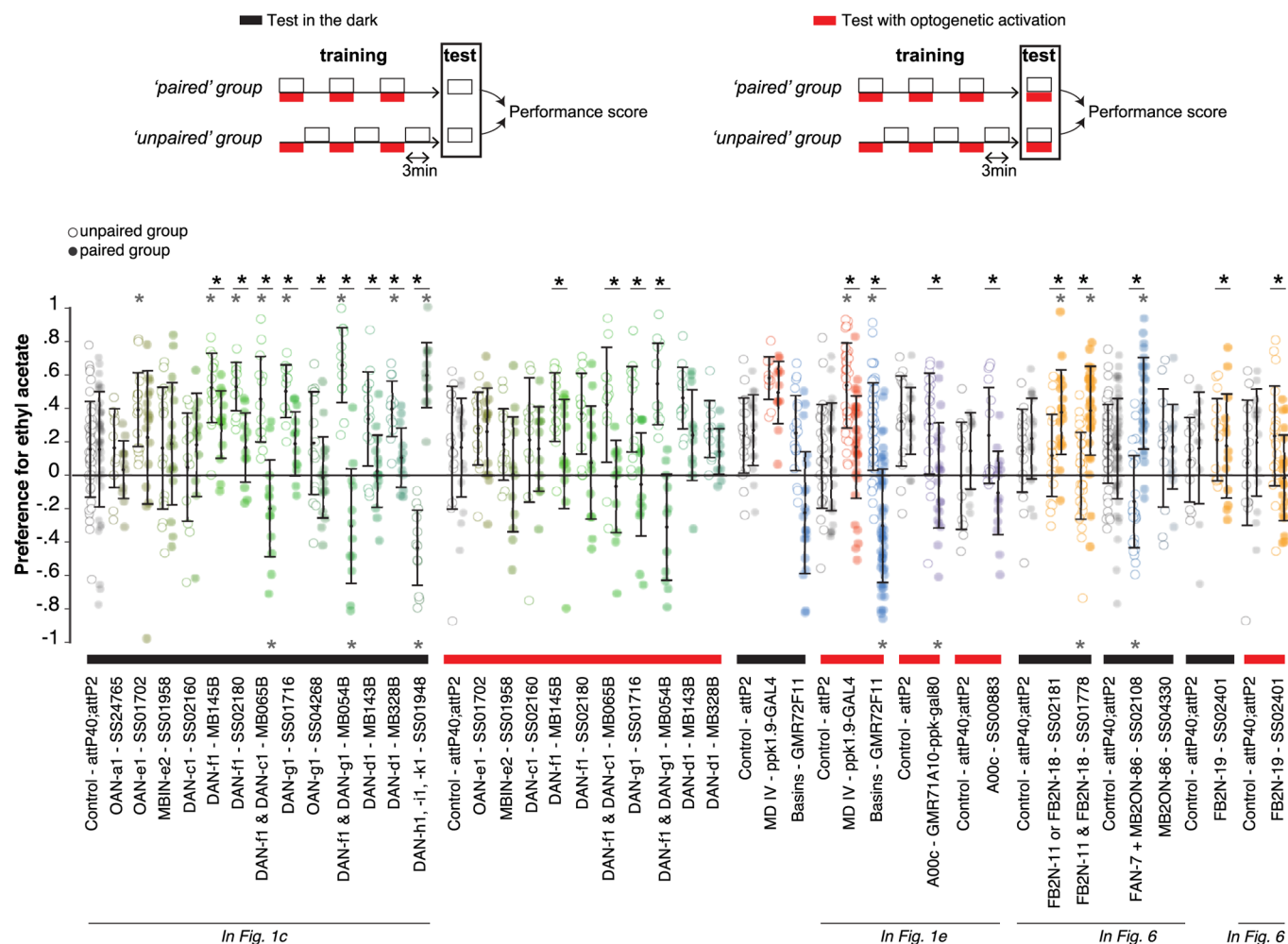
Correspondence and requests for materials should be addressed to A.L.-K., A.C. or M.Z.

Peer review information *Nature Neuroscience* thanks Rachel Wilson and the other, anonymous, reviewer(s) for their contribution to the peer review of this work.

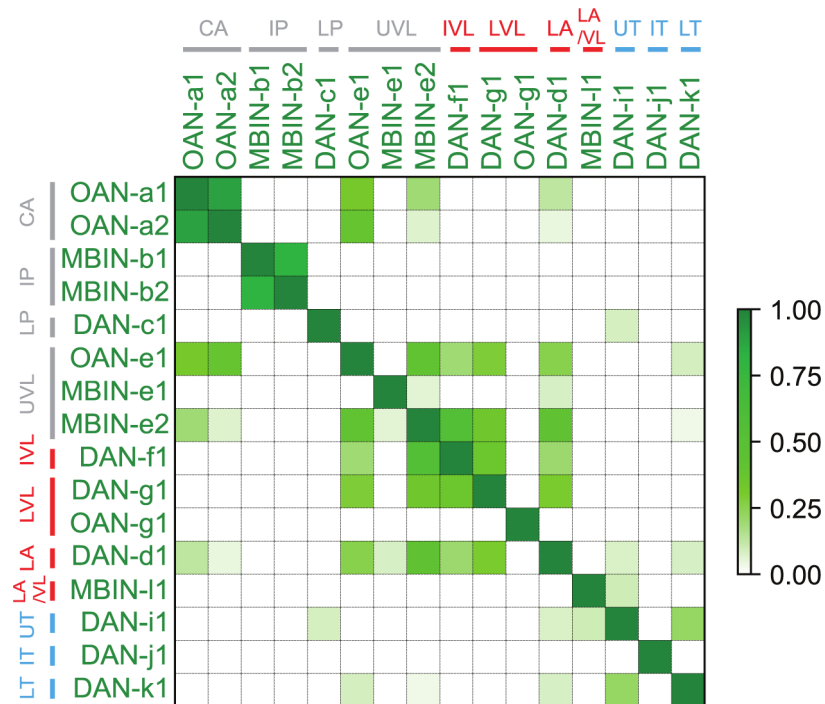
Reprints and permissions information is available at www.nature.com/reprints.



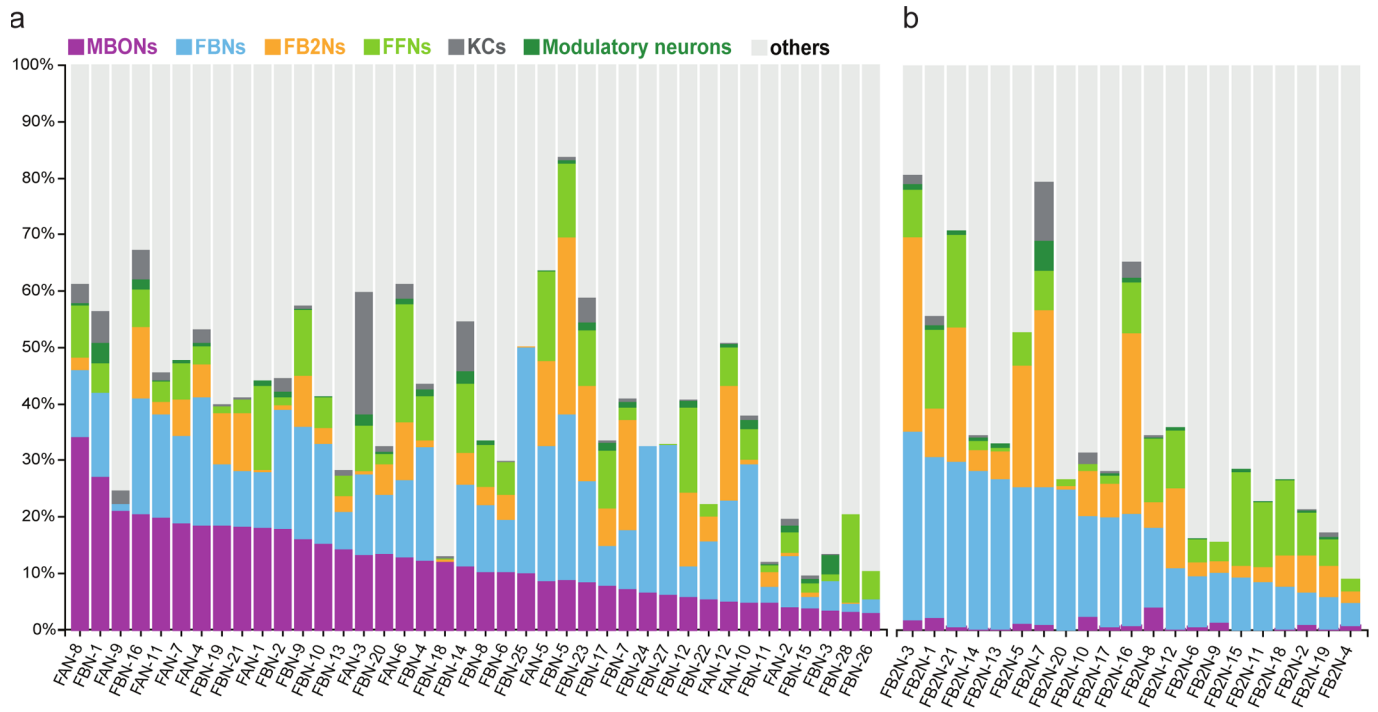
Extended Data Fig. 1 | Expression patterns of Split-GAL4 lines. Each panel shows a representative confocal maximum intensity projection (out of $N=3$) of the complete CNS of third-instar larvae (indicated by the *dotted line* in the first panel), with the neuropil labeled with anti-N-Cad antibody (*blue*) and the Split-GAL4 line expression pattern revealed with *UAS-myr-GFP* (*green*). Arrowheads indicate cell bodies of identified neurons.



Extended Data Fig. 2 | Detailed characterization of associative memories formed through different kinds of ‘optogenetic punishments’ or ‘optogenetic rewards’. Preference scores are shown for the trained odor, ethyl acetate, when it was paired (*paired group*, closed circles) or not paired (*unpaired group*, open circles) with optogenetic punishments or rewards. These Preference scores are used to compute the Learning Performance Scores as shown in Fig. 1c,e and 6a-c, additional testing conditions are also shown here. With some natural punishments, aversive memory is behaviorally expressed by trained *Drosophila* larvae only if the punishment is present at the moment of the test¹⁶. Here we assayed olfactory aversive memories in two ways: both with or without optogenetic punishment (red and black bars, respectively) during the retention test. Odor preference was decreased and increased, respectively, relative to genetic controls, after pairing the odor with the presence and absence of the following optogenetic punishments: co-activation of the aversive DAN-f1 and DAN-g1, co-activation of DAN-f1 and DAN-c1, or activation of Basins. Aversive memory formed by DAN activation (green) or by Basins activation (blue) was expressed to the same extent with or without the DANs activated during the retention test. However, memory evoked by the activation of nociceptive MD IV neurons (orange) or FB2N-19 (yellow) was fully expressed only if these neurons were active again during the retention test. Odor preference was increased and decreased, respectively, relative to genetic controls, after pairing the odor with the presence and absence of the following optogenetic rewards: the co-activation of DAN-h1, -i1, and -k1 (dark green); the activation of FB2N-18 and FB2N-11 (yellow), or activation of FAN-7 (blue-gray). Thus, both absence of odor in the unpaired group of animals, as well as the presence of odor in the paired group of animals can be associated with the activation of some DANs or some of their afferent neurons. These results suggest that presenting an odor unpaired with the activation of some of these DANs induces memory of opposite valence to the paired presentation. For other DANs or afferent neurons, only paired (for example A00c, purple) or only unpaired (for example the modulatory DAN-f1, the nociceptive MD IV sensory neuron, or FB2N-19) contingency significantly affected odor preference with respect to the control group. Either of these two observed types of effects can contribute to the negative or positive learning performance indexes plotted in Fig. 1c,e and 6a-c. Sample sizes: N = **42**, 11, 17, 16, 12, 14, 12, 13, 12, 16, 12, 14, 12, 12, 15, 14, 12, 11, 14, 13, 12, 14, 11, 11, 11, **18**, 11, 20, **25**, 33, 52, **14**, 21, **14**, 14, **18**, 18, 31, **52**, 27, 11, 11, 10, **13**, 20 (control groups in bold). Mean and standard deviations are shown. Black *: p-value < Holm-Bonferroni-adjusted threshold for 0.05 from a two-sided Wilcoxon signed rank test comparison between paired and unpaired group. Grey *: p-value < Holm-Bonferroni-adjusted threshold for 0.05 from a two-sided Mann-Whitney U test comparison between the preference scores for a given group (paired or unpaired) and the preference scores (for paired or unpaired protocol, respectively) obtained by the control line shown on the left of each set of data. Exact p-values are available in Source Data Fig. 1.



Extended Data Fig. 3 | Matrix of similarity between modulator neurons based on the amount of common input. We computed the cosine similarity of the connectivity matrix of row input neurons onto column modulatory neurons, which is the dot product of the rows, divided by the multiplication of the norm of each row. An input here is a connection, consisting typically of many synapses, from a specific cell type onto the modulatory neuron. Inputs onto a modulatory neuron are considered if the pair of left and right neurons presynaptic to the pair of left and right modulatory neurons is each above a threshold of 1% (for example the presynaptic neuron makes 3 synapses onto a neuron with 300 postsynaptic sites) and the sum of both is over 3.3% (for example the sum of both connections is above 10 synapses for receiving neurons with 300 postsynaptic sites). Interestingly, functionally similar DANs, whose activation leads to aversive memory for paired odors share a higher fraction of presynaptic partners with each other than with other DANs. By contrast some modulatory neurons that innervate the same compartment but express different neurotransmitters (for example OAN-g1 and DAN-g1) receive inputs from drastically different subsets of pre-modulatory neurons. Such modulatory neurons that innervate the same compartment could therefore be differentially recruited during learning. Interestingly though, OAN-e1 and MBIN-e2 in the UVL, whose activation paired with odor did not induce memory in our paradigm and that were not significantly activated by fictive punishments share a higher fraction of their input with the VL/LA DANs than with other modulatory neurons. This raises the possibility that the UVL modulatory neurons may be recruited by similar stimuli to the VL/LA DANs, but only in specific circumstances.



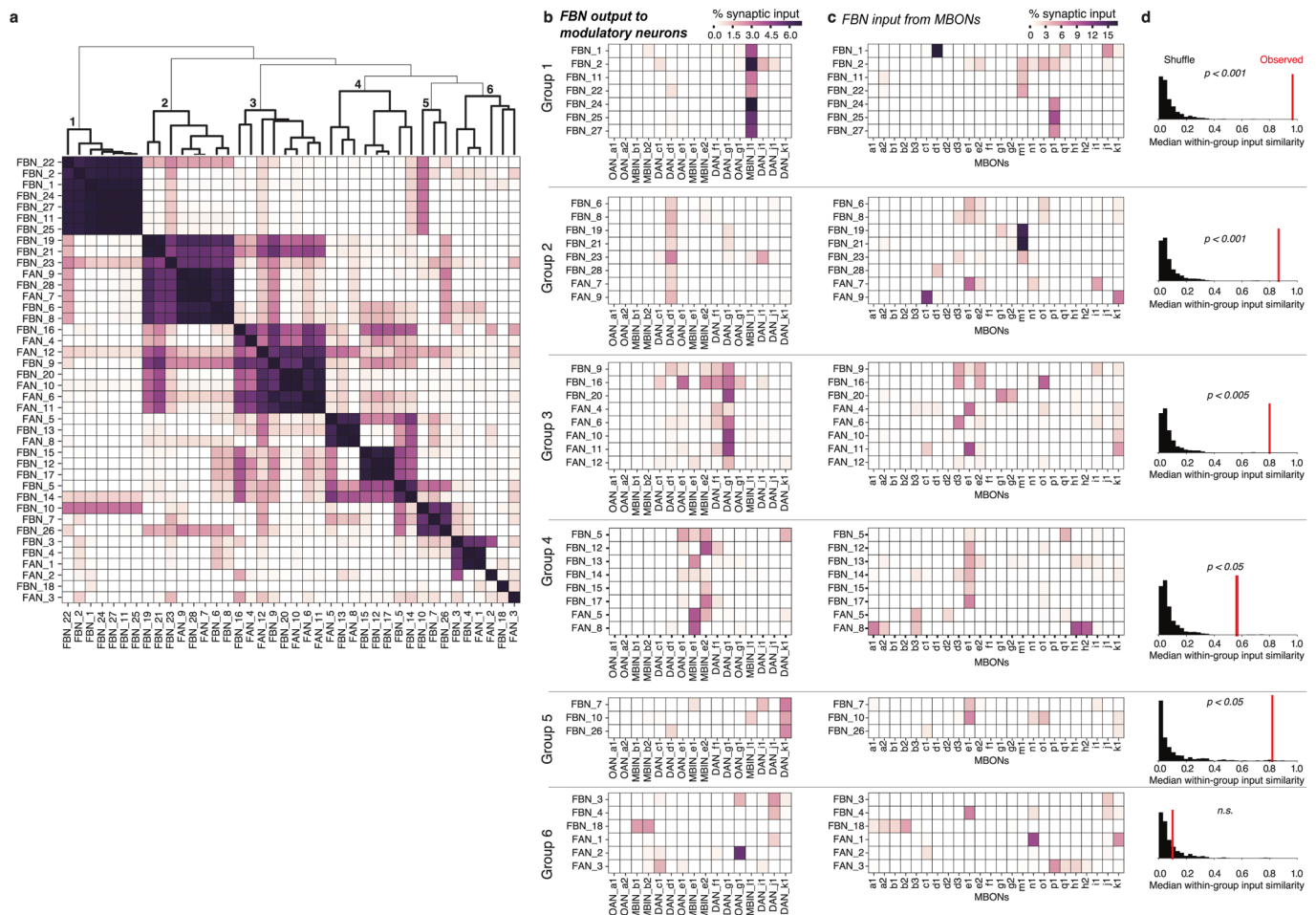
c

	FAN-8 [#2]	FAN-9 [#2]	FAN-16 [#2]	FAN-7 [#2]	FAN-4 [#2]	FAN-19 [#2]	FAN-1 [#2]	FAN-2 [#2]	FAN-9 [#2]	FAN-10 [#2]	FAN-13 [#2]	FAN-3 [#2]	FAN-20 [#2]	FAN-6 [#2]	FAN-4 [#2]	FAN-18 [#2]	FAN-14 [#2]	FAN-8 [#2]	FAN-5 [#2]	FAN-3 [#2]	FAN-17 [#2]	FAN-7 [#2]	FAN-24 [#2]	FAN-27 [#2]	FAN-12 [#2]	FAN-22 [#2]	FAN-12 [#2]	FAN-10 [#2]	FAN-11 [#2]	FAN-2 [#2]	FAN-15 [#2]	FAN-9 [#2]	FAN-3 [#2]	FAN-28 [#2]	FAN-26 [#2]	average						
MBONs	34	27	21	21	20	19	19	19	18	18	18	18	13	13	13	12	12	11	10	10	10	9	9	24	29	18	18	25	3	5	4	4	4	4	3	3	12.1					
FBNs	12	15	1	21	18	15	23	11	10	20	11	14	20	0	6	3	4	4	15	31	17	7	11	26	26	5	10	18	25	3	9	2	5	2	2	13.9						
FB2Ns	2	0	0	13	2	6	6	9	3	0	1	9	3	3	0	0	6	3	4	0	15	31	17	7	19	0	13	4	20	1	3	1	1	0	0	0	5.7					
FFNs	9	5	0	7	4	6	3	1	2	15	2	12	5	4	8	2	21	8	0	12	7	6	0	16	13	10	10	10	2	0	0	15	2	7	6	1	4	2	1	16	5	6.2
MBIN	0	4	0	2	0	1	0	0	1	1	0	0	2	0	1	1	0	2	1	0	0	0	1	1	1	1	1	1	1	1	1	1	3	0	0	0	0	0.8				
KCs	3	6	3	5	2	0	2	0	0	0	0	2	1	0	2	1	0	1	22	1	3	1	0	2	1	0	0	0	0	0	0	1	0	1	0	0	0	0	1.8			
others	39	43	75	33	54	52	47	60	59	56	55	42	58	72	40	67	39	56	87	45	66	70	50	36	16	41	66	59	67	67	59	78	49	62	88	80	90	86	79	90	59.5	

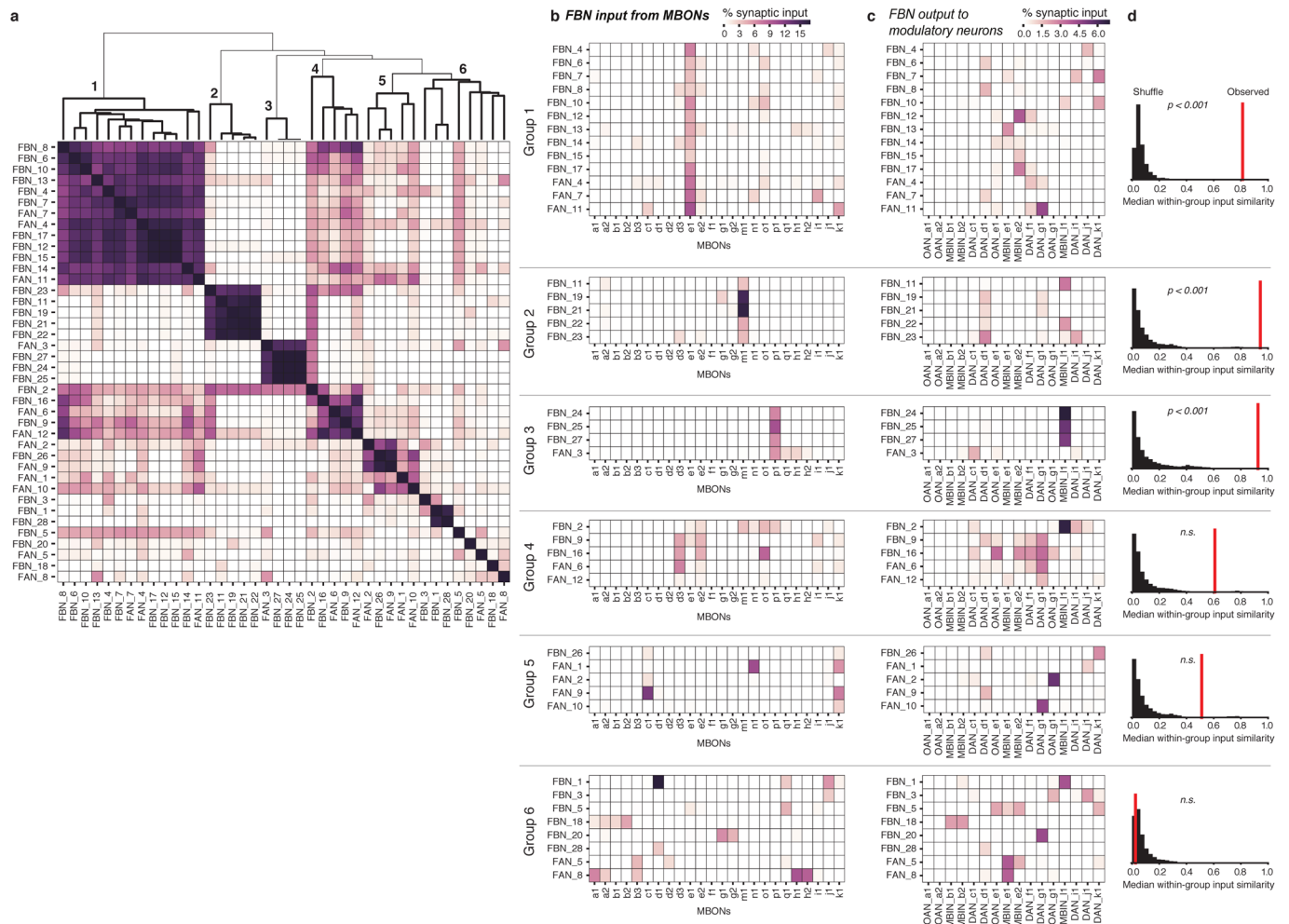
	FB2N-3 [#2]	FB2N-1 [#2]	FB2N-21 [#2]	FB2N-14 [#2]	FB2N-13 [#2]	FB2N-5 [#2]	FB2N-7 [#2]	FB2N-20 [#2]	FB2N-10 [#2]	FB2N-17 [#2]	FB2N-16 [#2]	FB2N-8 [#2]	FB2N-12 [#2]	FB2N-6 [#2]	FB2N-9 [#2]	FB2N-15 [#2]	FB2N-11 [#2]	FB2N-18 [#2]	FB2N-2 [#2]	FB2N-19 [#2]	FB2N-4 [#2]	average	
MBONs	2	2	1	0	0	1	1	0	3	1	1	4	0	1	1	0	0	0	0	1	0	1	1.0
FBNs	33	29	29	28	27	24	24	25	18	19	20	14	11	9	9	9	8	6	6	6	4	17.2	
FB2Ns	34	9	24	4	5	22	31	1	8	6	32	4	14	2	2	2	3	5	7	6	2	10.6	
FFNs	8	14	17	2	1	6	7	1	1	1	9	11	10	4	3	17	11	13	8	5	2	7.3	
MBIN	1	1	1	1	1	0	5	0	0	0	1	0	1	0	0	1	0	0	1	0	0	0.6	
KCs	2	2	0	0	0	0	10	0	2	0	3	0	0	0	0	0	0	0	0	1	0	1.0	
others	19	44	29	65	67	47	20	73	68	72	35	65	64	84	84	71	77	73	78	83	91	62.3	

Extended Data Fig. 4 | Input onto feedback neurons. Figure shows the fractions of total dendritic input each pre-modulatory neuron (FBN, FB2N or FFN) receives from KCs, modulatory neurons, MBONs, FBNs, FB2Ns, FFNs, and from other non-MB neurons (others). **a** FBNs receive on average 12% of their inputs directly from MBONs and most of them also receive inputs from other FBNs, with an average of 26% from MBONs and other FBNs combined (see also Supplementary Figure 4a). **b** FB2Ns receive inputs both from FBNs (on average 17%) and from other FB2Ns (on average 28% from FBNs and FB2Ns combined). Many feedback neurons also receive a significant fraction of input from other unknown neurons from other brain areas (other than MB), suggesting that the feedback about the learnt valences of stimuli is integrated with or modulated by other information. **c** Tables show percent of inputs onto FBNs (*top*) and FB2Ns (*bottom*) from MBONs, FBNs, FB2Ns, FFNs, modulatory neurons and Kenyon cells.

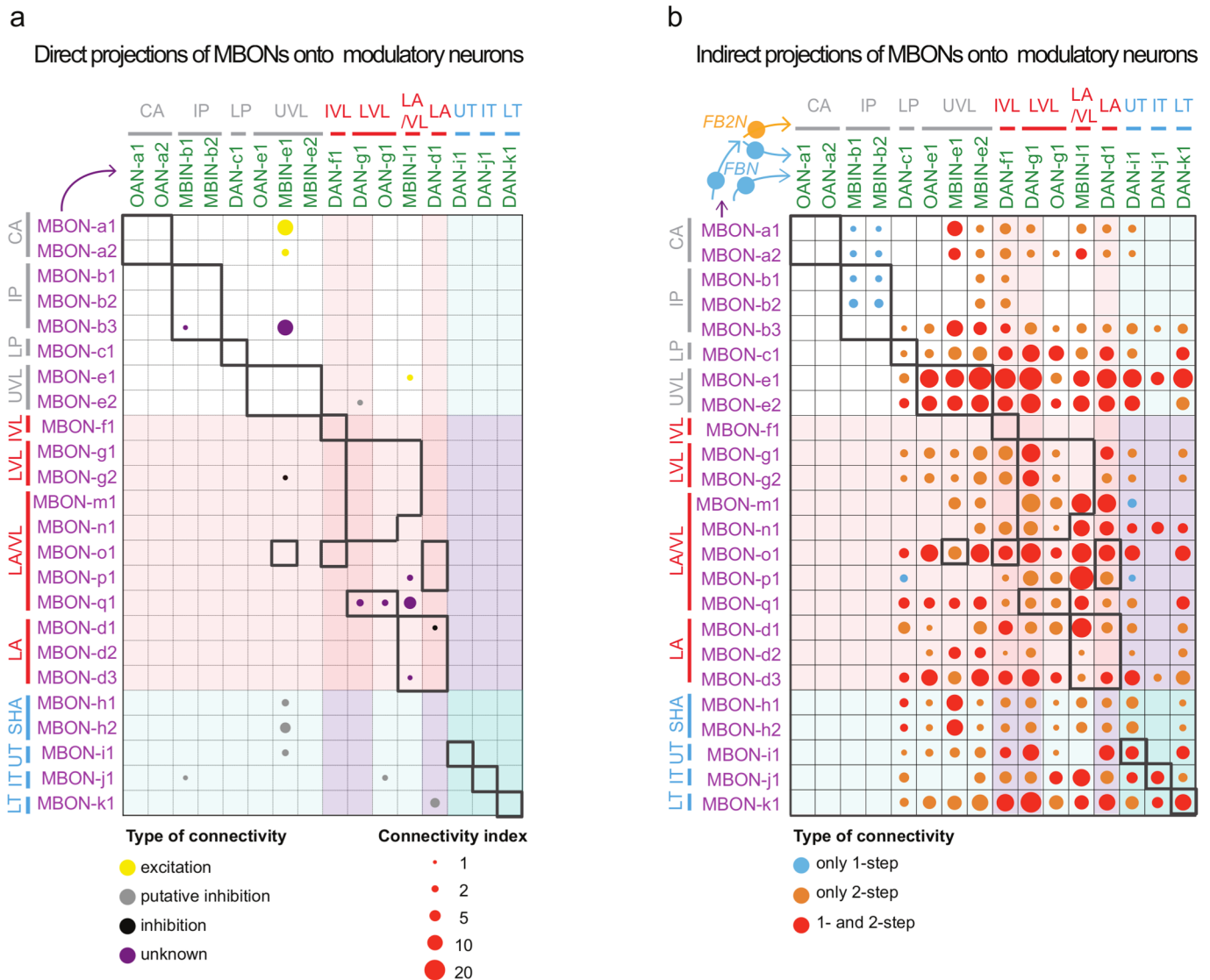
Extended Data Fig. 5 | (related to Fig. 3a) Modulatory neurons receive convergent one-step feedback from multiple MBONs from functionally distinct compartments. Connectivity of each of the 40 feedback neuron (FBN) pairs that provide one-step feedback from MBONs to DANs. Each diagram represents the connectivity of a single left-right pair of homologous FBNs. Each box indicates a separate compartment. *Purple*, compartment(s) of the presynaptic MBON(s). *Green*, compartment(s) of the postsynaptic modulatory neuron(s). FBNs are ordered according to the modulatory neuron they innervate, starting with peduncle modulatory neurons and ending with the medial lobe ones. Classical neurotransmitter profiles of the MBONs and FBNs are indicated by the arrow (cholinergic, excitatory connection), vertical line (GABAergic, inhibitory connection) or square (glutamatergic, probably also inhibitory connection) for the neurons for which they are known from immunostaining (For images, see Extended Data Fig. 9 for FBNs and ref. 12 for MBONs), or by a circle when they are unknown. 7 FBNs provide exclusively within-compartment feedback. 13 FBNs provide exclusively cross-compartment feedback (named FANs, for feed-across). 8 FBNs synapse onto multiple modulatory neurons from multiple compartments. The largest class of FBNs (17) receives input from multiple MBONs, with the majority (at least 13) receiving input of potentially opposite sign from MBONs from functionally distinct compartments. More than a quarter of FBNs (at least 12) receive direct GABAergic (inhibitory) or glutamatergic (also potentially inhibitory) input from MBONs from one compartment and direct cholinergic (excitatory) input from MBONs from a functionally distinct compartments enabling them to compare the odor drive to these MBONs. Many DANs (DAN-f1, d1, i1, j1, and k1) receive potentially inhibitory (excitatory FBN downstream of an inhibitory MBON) one-step feedback from MBONs from one compartment and potentially disinhibitory (inhibitory FBN downstream of an inhibitory MBON) or excitatory (excitatory FBN downstream of an excitatory MBON) one-step feedback from MBONs from a functionally distinct compartment. A common pattern for the lobe DANs implicated in memory formation may be a likely inhibitory connection from an MBON from their own compartment and a likely disinhibitory connection from an MBON from a compartment of opposite valence (observed for both DAN-g1 and i1), that could enable these DANs to compare the odor drive to MBONs from compartments of opposite valence.



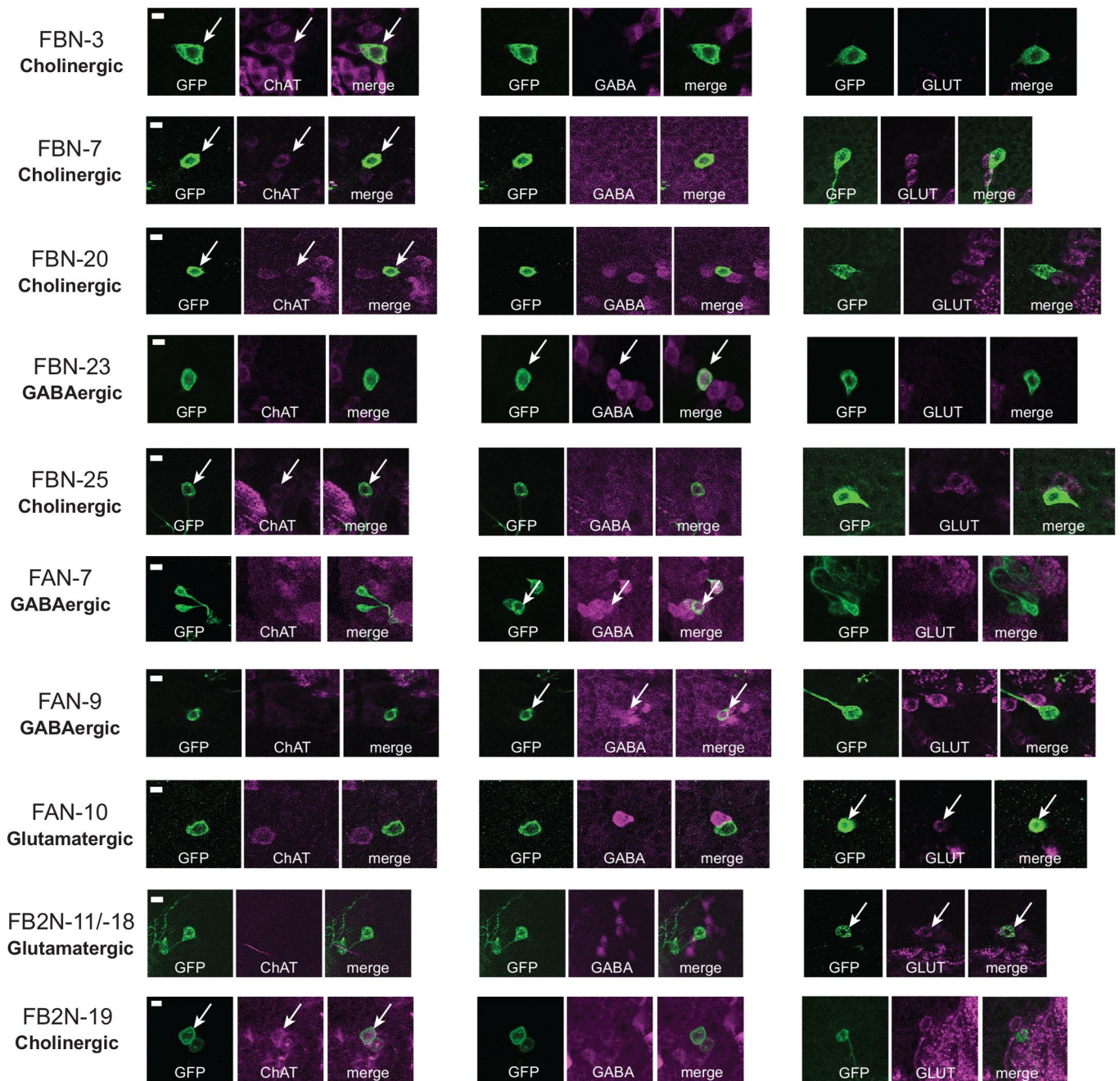
Extended Data Fig. 6 | Clustering FBNs based on input from MBONs. **a** Heat map of FBN similarity based on the pattern of FBN synaptic inputs from MBONs. The similarity between a pair of FBNs was computed as the cosine similarity between the vectors of their normalized synaptic inputs from all MBONs. Indices were ordered by agglomerative clustering with average linkage (*dendrogram* shown at top). We highlight six groups of FBNs defined by similarities in their input patterns (*bold lines in dendrogram*, numbered). **b** Heat maps showing patterns of input from MBONs onto FBNs for the input groups highlighted in **a**. In all cases, connectivity is measured in a Heat map of FBN similarity based on the pattern of FBN synaptic inputs from MBONs. The similarity between a pair of FBNs was computed as the cosine similarity between the vectors of their normalized synaptic inputs from all MBONs. Indices were ordered by agglomerative clustering with average linkage (*dendrogram* shown at top). We highlight six groups of FBNs defined by similarities in their input patterns (*bold lines in dendrogram*, numbered). **c** Heat maps showing patterns of synaptic output from FBNs to modulatory neurons for the input groups highlighted in **a**. In all cases, connectivity is measured in normalized synaptic input on the postsynaptic neuron. Most input groups receive dominant input from a single specific MBON (Groups 1,2, 5) or small group of MBONs (Groups 3 and 4), while Group 6 is not well-clustered and contains a variety of dissimilar input patterns. **d** The observed similarity in the output patterns between FBNs within each group, compared to shuffled data. For each group clustered by input pattern, we computed the observed median of cosine similarity of the output vectors across all pairs of neurons (*red line*). In Groups 1,2, and 3, the neurons clustered by inputs had more similar output patterns than would be expected by chance. To determine significance, we compared the observed similarity to the distribution of the median cosine similarity for randomly permuted samples from the observed population of input vectors (*black histograms*, $n=10000$ randomized trials) with a one-sided permutation test. A Holm-Sidak correction was applied to p -values to correct for multiple comparisons. *n.s.*: $p > 0.05$.



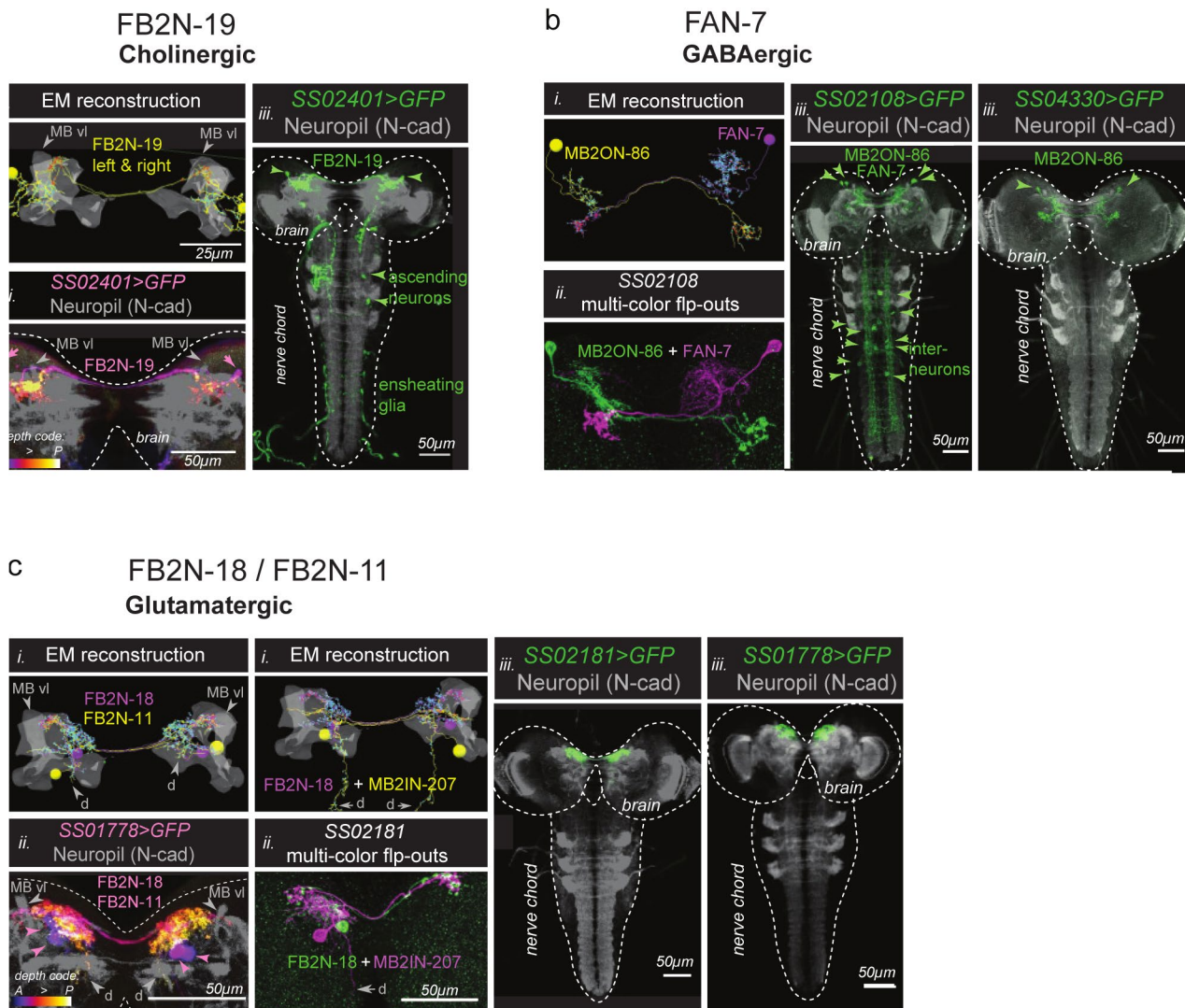
Extended Data Fig. 7 | Clustering FBNs based on output onto modulatory neurons. **a** Heat map of FBN similarity based on the pattern of FBN synaptic output across all modulatory neurons. The similarity between a pair of FBNs was computed as the cosine similarity between the vectors of normalized synaptic output onto all modulatory neurons. Indices were ordered by agglomerative clustering with average linkage (*dendrogram shown at top*). We highlight six groups of FBNs defined by similarities in their output patterns (*bold lines in dendrogram, numbered*). **b** Heat maps showing patterns of synaptic output from FBNs to modulatory neurons for output groups highlighted in **a**. Each group corresponds to several FBNs strongly targeting one or a small number of modulatory neurons, suggesting that some modulatory neurons are more strongly modulated than others. **c** Heat maps showing patterns of input onto FBNs from MBONs for the output groups highlighted in **a**. **d** The observed similarity in the input patterns between FBNs within each group, compared to shuffled data. For each group (as defined by output patterns), we computed the observed median of cosine similarity of the input vectors across all pairs of neurons (*red line*). In Groups 1-5, the neurons clustered by outputs had more input output patterns than would be expected by chance. To determine significance, we compared the observed similarity to the distribution of the median cosine similarity for randomly permuted samples from the observed population of input vectors (*black histograms, n=10000 randomized trials*) with a one-sided permutation test. A Holm-Sidak correction was applied to p-values to correct for multiple comparisons. *n.s.*: $p > 0.05$.



Extended Data Fig. 8 | Direct MBONs to modulatory neuron connectivity is very sparse, in contrast to the very dense connectivity via one- and two-step feedback pathways. a Connectivity matrix showing normalized synaptic input (expressed as % input) each modulatory neuron (*columns*) receives from each MBON (*rows*). Only reliable connections for which the postsynaptic neuron receives at least 1% of input from the presynaptic neuron are shown. When the neurotransmitter of the MBON is known, the circle is color-coded to represent type of connection: excitatory (ChAT) or probably disinhibitory (GluT). Color shades represent the valence of the memory formed in a given compartment (red: aversive memory, blue: appetitive memory). True within-compartment feedback connections from an MBON that receives direct synaptic input from that modulatory neuron are boxed in bold. Very few modulatory neurons receive direct input from MBONs, in contrast to the dense connectivity between MBONs and modulatory neurons via the indirect one- and two-step feedback pathways (*b*). **b** Connectivity matrix showing indirect connections between MBONs and modulatory neurons via one-step and/or two-step feedback pathways. The matrix was obtained by summing the matrices from Fig. 3b and Fig. 5e. The color indicates the type of indirect connection existing between a given MBON and a given DAN. Bubble size represents a connectivity index computed as in Fig. 3b and Fig. 5e. A connectivity index of 1 or 10 means that for all connections comprising that indirect feedback pathway the presynaptic neuron accounts for 1% and 10% of input onto that postsynaptic neuron, respectively. One- and two-step feedback drastically increases the connectivity between MBONs and modulatory neurons, compared to direct connections (*a*).



Extended Data Fig. 9 | Identification of neurotransmitters expressed in some FBNs/FB2Ns. Neurotransmitter expression detected in neuron somata using antibody labelling. We identified GAL4 lines that drive gene expression in some of the FBN or FB2N neurons and used them to express GFP in these neurons. We stained central nervous systems with antibodies against GFP and either ChAT (choline acetyltransferase), GABA (gamma aminobutyric acid) or GLUT (vesicular glutamate transporter). Each row shows from left to right: the name of the individual neuron, anti-GFP (green), anti-ChAT (magenta), and both antibody stainings combined; anti-GFP (green), anti-GABA (magenta), and both antibody stainings combined; anti-GFP (green) and anti-GLUT (magenta), and both antibody stainings combined. Whether a cell is cholinergic, GABAergic or glutamatergic is listed at the beginning of each row under the neuron name. Images show confocal maximum intensity projections of specific neuronal cell bodies. At least two replicates were obtained per genotype. Scale bars: 5 μ m.



Extended Data Fig. 10 | (related to Fig. 6) Identification of driver lines for EM-reconstructed Feedback neurons. We were able to generate Split-GAL4 lines that drive expression in a single pair of neurons, or in very few cell types, for three different pairs of FBNs or FB2Ns that target VL DANs (**a-c**). We used these lines to optogenetically activate these neurons instead of a US during an associative learning paradigm (Fig. 6). **i**) Skeletons of specific feedback neurons reconstructed in the EM. Red dots, presynaptic sites. Blue dots, postsynaptic sites. Grey, mushroom body vertical lobe (MB vl) for reference. *d*, dendritic arbor. **ii**) Maximum intensity projections of confocal stacks of larval brains showing the same neurons visualized with reporters targeted using specific Split-GAL4 lines. For some lines multicolor flip-outs were used to visualize each neuron in a different color to facilitate identification and comparison with EM (N=1). Grey, neuropil visualized with N-cad. *Dashed line*, brain outline. **iii**) Maximum intensity projections of confocal stacks of the entire nervous system showing the complete expression pattern of each line revealed by driving *UAS-myr-GFP*. Grey, neuropil visualized with N-cad. *Dashed line*, nervous system outline. Representative image from N=3. **a**, The *SS02401-Split-GAL4* line drives expression in FB2N-19 (**i**) in the brain (**ii**), and very weakly and stochastically (not reproducibly in all samples) in a few ascending neurons and ensheathing glia in the nerve cord (**iii**). **b**, The *SS02108-Split-GAL4* line drives expression in FAN-7 and MB2ON-86 (**i**) in the brain visualized with multicolor flip-outs in (**ii**). Complete expression pattern of *SS02108-Split-GAL4* visualized with *UAS-myr-GFP* shows additional expression in a few somatosensory interneurons in the nerve cord, called ladders, that mediate avoidance behavior and are hence unlikely to have a positive valence and evoke the appetitive memory observed in Fig. 6b. We identified the *SS04330-Split-GAL4* line as driving expression specifically in the MB2ON-86 neuron and used it as an additional control in Fig. 6b. **c**, The *SS01778-Split-GAL4* line drives expression in both FB2N-18 and FB2N-11, which have very similar morphology and very similar connectivity (Supplementary Figures 3 and 4b-d). The *SS02181-Split-GAL4* line (**ii** shows multi-color flip-outs) drives expression in FB2N-18 and in MB2IN-207, one of the weakly connected pre-modulatory neurons from lineage DAMv12. Notice the ventrally projecting dendrite (*d*), a distinctive feature of MB2IN-207 neuron (**i**). *UAS-myr-GFP* expression patterns of the two lines show that they do not drive expression in any other neurons in the nerve cord (**iii**).

Reporting Summary

Nature Research wishes to improve the reproducibility of the work that we publish. This form provides structure for consistency and transparency in reporting. For further information on Nature Research policies, see [Authors & Referees](#) and the [Editorial Policy Checklist](#).

Statistics

For all statistical analyses, confirm that the following items are present in the figure legend, table legend, main text, or Methods section.

n/a Confirmed

- The exact sample size (n) for each experimental group/condition, given as a discrete number and unit of measurement
- A statement on whether measurements were taken from distinct samples or whether the same sample was measured repeatedly
- The statistical test(s) used AND whether they are one- or two-sided
Only common tests should be described solely by name; describe more complex techniques in the Methods section.
- A description of all covariates tested
- A description of any assumptions or corrections, such as tests of normality and adjustment for multiple comparisons
- A full description of the statistical parameters including central tendency (e.g. means) or other basic estimates (e.g. regression coefficient) AND variation (e.g. standard deviation) or associated estimates of uncertainty (e.g. confidence intervals)
- For null hypothesis testing, the test statistic (e.g. F , t , r) with confidence intervals, effect sizes, degrees of freedom and P value noted
Give P values as exact values whenever suitable.
- For Bayesian analysis, information on the choice of priors and Markov chain Monte Carlo settings
- For hierarchical and complex designs, identification of the appropriate level for tests and full reporting of outcomes
- Estimates of effect sizes (e.g. Cohen's d , Pearson's r), indicating how they were calculated

Our web collection on [statistics for biologists](#) contains articles on many of the points above.

Software and code

Policy information about [availability of computer code](#)

Data collection

Fiji 1.0 (<http://fiji.sc>), CATMAID (<http://github.com/catmaid/catmaid/>), PyTorch (1.1.0. <https://pytorch.org/>)

Data analysis

R 3.5.3 (<https://www.r-project.org/>), Matlab R2017a (The Mathworks, Inc) and CATMAID's built-in analytical tool trackEM2 were used to analyse connectome data. Matlab R2017a was also used to analyze behavioral, imaging data. Fiji 1.0. was used to analyze imaging data. Clampex 10.4 was used to analyse electrophysiological data. Hierarchical clustering on the similarity matrix was done with Scipy. Model used Python 3.7.3 (<https://www.python.org/>) and PyTorch 1.1.0.

For manuscripts utilizing custom algorithms or software that are central to the research but not yet described in published literature, software must be made available to editors/reviewers. We strongly encourage code deposition in a community repository (e.g. GitHub). See the Nature Research [guidelines for submitting code & software](#) for further information.

Data

Policy information about [availability of data](#)

All manuscripts must include a [data availability statement](#). This statement should provide the following information, where applicable:

- Accession codes, unique identifiers, or web links for publicly available datasets
- A list of figures that have associated raw data
- A description of any restrictions on data availability

All electron microscopy data is available online, e.g. at the NeuroData.io website and the Virtual Fly Brain website (http://www.virtualflybrain.org/site/vfb_site/home.htm).

The confocal stacks are available from the HHMI Janelia resource website.

Raw behavioral and imaging data is provided as supplementary data.

Field-specific reporting

Please select the one below that is the best fit for your research. If you are not sure, read the appropriate sections before making your selection.

Life sciences Behavioural & social sciences Ecological, evolutionary & environmental sciences

For a reference copy of the document with all sections, see [nature.com/documents/nr-reporting-summary-flat.pdf](https://www.nature.com/documents/nr-reporting-summary-flat.pdf)

Life sciences study design

All studies must disclose on these points even when the disclosure is negative.

Sample size	<p>For behavioral experiments, sample size is between 11 and 16. This sample size is used in similar studies and is sufficient to reach significance with the non-parametric tests we use (e.g. Saumweber et al, 2018). Empty lines were used as a negative controls and were generally tested at least once every day. The lines ppk1.9-GAL4 and 72F11-GAL4 were used as positive controls and were tested regularly throughout the screening and thus reached higher sample size.</p> <p>For calcium imaging experiments, sample size is between 5 and 14 for most dataset. This sample size is sufficient to reach significance with non-parametric tests and is commonly used in other imaging studies testing functional connectivity (e.g. Felseberg et al., 2017). A first batch of experiments was performed with three crosses (OAN-e1-, MBIN-e2- or DAN-f1-SplitGAL4 > UAS-GCamp6f / ppk1.9-LexA > LexAop-CsChrimson), and repeated later together with the rest of crosses, and were pooled, thus reaching a higher sample size.</p> <p>The sample size for patch-clamp recording is between 3 and 9, similar to other studies (e.g. Jovanic et al, 2016).</p>
Data exclusions	<p>The data obtained from calcium imaging with a specific cross (DAN-g1-SplitGAL4 > UAS-GCamp6f / ppk1.9-LexA > LexAop-CsChrimson) was excluded following the discovery of transvection in that cross and was regenerated using a method for spatially defined optogenetic stimulation, as described in the methods.</p> <p>These exclusion criteria were pre-established.</p>
Replication	<p>Behavior: When available, we tested many driver lines that drove expression in the same neurons: DAN-f1, DAN-d1, FB2IN-18, as seen in Figure 1c and 6h. Only attempts at replication that were successful are shown. Data that were not reproducible with driver lines covering the same neuron of interest were excluded.</p> <p>Calcium imaging: We tested two lines for DAN-f1 and DAN-d1 and had qualitatively similar results (data shown for only one driver for each neuron). Thus, the attempts at replication were successful.</p>
Randomization	<p>Behavior: The order of the sequence of presentation for odor and light stimulation (i.e. for paired group: half training protocols are in the sequence odor+/air-/odor+/air-/odor+/air- and half are air-/odor+/air-/odor+/air-/odor+, same logic for unpaired group) was alternated throughout all experiments. For each figure, the driver lines tested were done so in a random maner, i.e. each line was tested everyday day when possible, the time of the day was also shuffled among the lines tested. Most experiments were done by a single experimenter, some additional data was obtained by a second experimenter who regularly tested the negative and positive controls besides the neurons of interest.</p> <p>Calcium imaging: As many different crosses were tested in the same day, in a shuffled sequence, avoiding the same cross to be tested twice in a row.</p>
Blinding	<p>Behavior: All genotypes tested were coded to the experimenter.</p> <p>Calcium imaging: The genotypes were known by the experimenter, as the expression of tagged CsChrimson and GCamp6f in the different neurons was recognisable.</p>

Reporting for specific materials, systems and methods

We require information from authors about some types of materials, experimental systems and methods used in many studies. Here, indicate whether each material, system or method listed is relevant to your study. If you are not sure if a list item applies to your research, read the appropriate section before selecting a response.

Materials & experimental systems

n/a	Involved in the study
<input type="checkbox"/>	<input checked="" type="checkbox"/> Antibodies
<input checked="" type="checkbox"/>	<input type="checkbox"/> Eukaryotic cell lines
<input checked="" type="checkbox"/>	<input type="checkbox"/> Palaeontology
<input type="checkbox"/>	<input checked="" type="checkbox"/> Animals and other organisms
<input checked="" type="checkbox"/>	<input type="checkbox"/> Human research participants
<input checked="" type="checkbox"/>	<input type="checkbox"/> Clinical data

Methods

n/a	Involved in the study
<input checked="" type="checkbox"/>	<input type="checkbox"/> ChIP-seq
<input checked="" type="checkbox"/>	<input type="checkbox"/> Flow cytometry
<input checked="" type="checkbox"/>	<input type="checkbox"/> MRI-based neuroimaging

Antibodies

Antibodies used

Primary antibodies:
rabbit anti-GFP (cat# Af2020, Frontier Institute; 1:1000), chick anti-GFP (ab13970, abcam, 1:1000), rabbit anti-GABA (A2052,

Sigma; 1:100), mouse anti-ChAT (ChAT4B1, DSHB Hybridoma Product deposited by P.M. Salvaterra; 1:50), rabbit anti-DVGlut (Daniels et al., 2008, diluted 1:1000).

Secondary antibodies:

Alexa Fluor 568-conjugated goat anti-rabbit IgG (A-11036, Invitrogen Molecular Probes; 1:300),

Alexa Fluor 633-conjugated goat anti-mouse IgG (A-21050, Invitrogen Molecular Probes; 1:300),

Alexa Fluor 488-conjugated goat anti-chicken IgG (A-11039, Invitrogen Molecular Probes; 1:300).

Validation

rabbit anti-GFP: Immunohistochemistry in mouse (Takasaki et al., 2010), used in *Drosophila* (Fushiki et al., 2016)

chick anti-GFP: Immunohistochemistry-Wholemout in *Drosophila*

rabbit anti-GABA: Immunohistochemistry in *Drosophila*

mouse anti-ChAT: Immunohistochemistry in *Drosophila*

rabbit anti-DVGlut: Immunohistochemistry in *Drosophila* (Daniels et al., 2008)

Animals and other organisms

Policy information about [studies involving animals](#); [ARRIVE guidelines](#) recommended for reporting animal research

Laboratory animals

Drosophila melanogaster larvae, both sexes, third-instar stage (3.5 days old) were used. Strains are: SS24765-Split-GAL4, SS02160-Split-GAL4, SS01702-Split-GAL4, SS01958-Split-GAL4, SS02180-Split-GAL4, MB145B-Split-GAL4, MB065B-Split-GAL4 (Aso et al. 2014), S01716-Split-GAL4 (Saumweber et al. 2018), SS04268-Split-GAL4, MB054B-Split-GAL4, MB143B-Split-GAL4, MB328B-Split-GAL4, SS01948-Split-GAL4, SS00864-Split-GAL4, SS02163-Split-GAL4, SS00883-Split-GAL4, SS01726-Split-GAL4, SS01778-Split-GAL4, SS02181-Split-GAL4, SS02108-Split-GAL4, SS02401-Split-GAL4, yw;;attP2 and yw;attP40;attP2 (Pfeiffer et al. 2010, Jenett et al.2012), ppk-1.9-GAL4 ; GMR72F11-GAL4 (Ohshima et al. 2015), GMR71A10-GAL4 (Ohshima et al. 2015), ppk-GAL80 (Yang et al. 2009), repo-GAL80 (Awasaki et al. 2011), iav-LexA (Ohshima et al. 2015), GMR72F11-LexA (Jenett et al. 2012), ppk-1kb-hs43-lexA-GAD10, 58E02-LexAp65 (Liu et al. 2012) 20xUAS-IVS-GCaMP6f 15.693 (Chen et al. 2013), 13xLexAop2-IVS-GCaMP6f-p10 15.693 (BDSC 44276), 20xUAS-CsChrimson-mVenus (BDSC 55134), 13xLexAop2-CsChrimson-tdTomato (BDSC 55138), 20xUAS-CsChrimson-mCherry (Klapeetke et al. 2014), pJFRC29-10xUAS-IVS-myr::GFP-p10 (Pfeiffer et al. 2012)

Wild animals

None.

Field-collected samples

None.

Ethics oversight

Ethics oversight is not required for *Drosophila* investigations.

Note that full information on the approval of the study protocol must also be provided in the manuscript.